Development 140, 4386-4397 (2013) doi:10.1242/dev.098046

Mouse *Hoxa2* mutations provide a model for microtia and auricle duplication

Maryline Minoux[1,2], Claudius F. Kratochwil[1,3], Sébastien Ducret[1], Shilu Amin[4], Taro Kitazawa[5], Hiroki Kurihara[5], Nicoletta Bobola[4], Nathalie Vilain[1] and Filippo M. Rijli[1,3,*]

SUMMARY

External ear abnormalities are frequent in newborns ranging from microtia to partial auricle duplication. Little is known about the molecular mechanisms orchestrating external ear morphogenesis. In humans, *HOXA2* partial loss of function induces a bilateral microtia associated with an abnormal shape of the auricle. In mice, *Hoxa2* inactivation at early gestational stages results in external auditory canal (EAC) duplication and absence of the auricle, whereas its late inactivation results in a hypomorphic auricle, mimicking the human *HOXA2* mutant condition. By genetic fate mapping we found that the mouse auricle (or pinna) derives from the *Hoxa2*-expressing neural crest-derived mesenchyme of the second pharyngeal arch, and not from a composite of first and second arch mesenchyme as previously proposed based on morphological observation of human embryos. Moreover, the mouse EAC is entirely lined by *Hoxa2*-negative first arch mesenchyme and does not develop at the first pharyngeal cleft, as previously assumed. Conditional ectopic *Hoxa2* expression in first arch neural crest is sufficient to induce a complete duplication of the pinna and a loss of the EAC, suggesting transformation of the first arch neural crest-derived mesenchyme lining the EAC into an ectopic pinna. *Hoxa2* partly controls the morphogenesis of the pinna through the BMP signalling pathway and expression of *Eya1*, which in humans is involved in branchio-oto-renal syndrome. Thus, *Hoxa2* loss- and gain-of-function approaches in mice provide a suitable model to investigate the molecular aetiology of microtia and auricle duplication.

KEY WORDS: Hox, BMP, Craniofacial development, External auditory canal, Neural crest, Pharyngeal arch, Pinna, Auricle, External ear

INTRODUCTION

The external ear is composed of the auricle (or pinna) and the external auditory canal (EAC). A variety of factors can affect its morphogenesis, inducing a wide range of abnormalities such as microtia and partial auricle duplications (Alasti and Van Camp, 2009; Baschek et al., 2006; Gore et al., 2006; Hunter and Yotsuyanagi, 2005; Ku et al., 1998; Mishra and Misra, 1978; Pan et al., 2010). Microtia, which is characterised by a small, abnormally shaped auricle, is one of the most common external ear abnormalities; the estimated prevalence ranges from 0.8 to 4.2 per 10,000 births depending on the population (Alasti and Van Camp, 2009). External ear abnormalities can occur as the only clinical defect, but in most cases they appear in complex syndromes in which others organs and structures are affected. External ear anomalies are indeed commonly associated with internal and/or middle ear dysplasia, resulting in hearing loss and problems in speech and language development (Kountakis et al., 1995). Deciphering the molecular mechanisms involved in external ear morphogenesis is crucial not only to better understand the defaults affecting the external ear, but also to gain a more comprehensive view of the mechanisms involved in the genetic syndromes that encompass external ear abnormalities.

[1]Friedrich Miescher Institute for Biomedical Research, Maulbeerstrasse 66, CH-4058 Basel, Switzerland. [2]INSERM UMR 1121, Université de Strasbourg, Faculté de Chirurgie Dentaire, 1, place de l'hôpital, 67 000 Strasbourg, France. [3]University of Basel, CH-4056 Basel, Switzerland. [4]School of Dentistry, Faculty of Medical and Human Sciences, University of Manchester, Manchester M13 9PT, UK. [5]Department of Physiological Chemistry and Metabolism, Graduate School of Medicine, The University of Tokyo, 7-3-1 Hongo, Bunkyo-ku, Tokyo 113-0033, Japan.

*Author for correspondence (filippo.rijli@fmi.ch)

Accepted 19 August 2013

Genetic diagnostics in humans, as well as loss-of-function experiments in mice, have begun to identify signalling factors and transcriptional regulators involved in external ear morphogenesis. Among these factors, *Hoxa2* plays a crucial role. In humans, a *HOXA2* mutation induces a bilateral microtia associated with abnormal shape of the auricle (Alasti et al., 2008). Moreover, hearing impairment and partial cleft palate have been reported (Alasti et al., 2008). A role for *Hoxa2* in external ear morphogenesis is also observed in mice, where its inactivation induces duplication of the EAC and absence of the pinna (Gendron-Maguire et al., 1993; Mallo and Gridley, 1996; Mark et al., 1995; Rijli et al., 1993). This phenotype is associated with other craniofacial abnormalities, notably a cleft palate and middle ear structure malformations. Indeed, *Hoxa2* inactivation results in morphological transformation of the neural crest-derived skeletal elements of the second pharyngeal arch, including the middle ear ossicle stapes, into a duplicated set of first arch-like elements, including duplication of the middle ear ossicles malleus and incus (Gendron-Maguire et al., 1993; Rijli et al., 1993). By temporally controlled inactivation, we have further shown that pinna morphogenesis requires *Hoxa2* function through advanced developmental stages (Santagati et al., 2005). Whereas *Hoxa2* inactivation before E11.5 results in the absence of the pinna, *Hoxa2* inactivation at later stages (between E12.5 and E13.5) results in a hypomorphic pinna (Santagati et al., 2005), thus mimicking the human *HOXA2* mutant condition. Altogether, these data emphasize the major role of *Hoxa2* in auricle morphogenesis. However, the molecular programme that is regulated by *Hoxa2* is only beginning to be elucidated (Donaldson et al., 2012) and remains largely unknown. Furthermore, it is unclear whether *Hoxa2* is not only necessary but also sufficient to induce and orchestrate the whole developmental programme underlying pinna morphogenesis.

By genetic fate mapping, we show here that the mouse pinna derives from the second pharyngeal arch *Hoxa2*-expressing neural

crest cells (NCCs), and not from a combined contribution of first and second arch neural crest-derived mesenchyme, as proposed by some authors based on morphological observations of human embryos (reviewed by Hunter and Yotsuyanagi, 2005; Alasti and Van Camp, 2009; Klockars and Rautio, 2009; Passos-Bueno et al., 2009; Porter and Tan, 2005; Schoenwolf and Larsen, 2009). We further show that the mouse EAC is entirely lined by *Hoxa2*-negative first arch mesenchyme, and does not develop, as previously proposed, at the first pharyngeal cleft (Jakubíková et al., 2005; Schoenwolf and Larsen, 2009). By a conditional gain-of-function approach, we show that ectopic *Hoxa2* expression in first arch NCCs is alone sufficient to induce the transformation of the neural crest-derived first arch mesenchyme lining the EAC into a mirror-image duplication of the pinna. Functional and molecular analyses revealed that *Hoxa2* controls the formation of the pinna through the BMP signalling pathway by regulating the expression of bone morphogenetic protein 5 (*Bmp5*), *Bmp4* and twisted gastrulation (*Tsg*; *Twsg1* – Mouse Genome Informatics). Chromatin immunoprecipitation and parallel sequencing (ChIP-Seq) on second arch cells additionally shows that Hoxa2 binds to *Bmp4* and *Bmp5* non-coding regions, suggesting that they are direct targets. *Bmp5* inactivation results in a small pinna [known as the *short ear* mutation (King et al., 1994; Kingsley et al., 1992)], and we further show that *Bmp4* conditional inactivation also partially impairs pinna development. Moreover, *Hoxa2* regulates the expression of eyes absent 1 (*Eya1*), which in humans is involved in the branchio-oto-renal syndrome (Abdelhak et al., 1997; Kochhar et al., 2007). Thus, *Hoxa2* is a fundamental transcriptional regulator orchestrating the morphogenesis of the auricle. This genetic approach in the mouse might therefore represent a suitable model with which to understand the aetiology of human auricle abnormalities.

MATERIALS AND METHODS

Mouse lines and mating schemes

To fate map the external ear, the *Z/AP* (Lobe et al., 1999) and *Rosa-CAG-LSL-tdTomato* (Ai14) (Madisen et al., 2010) reporter mouse lines were crossed with the *R4::Cre* (Oury et al., 2006) mouse line. The $Hoxa2^{EGFP}$ and $Hoxa2^{EGFP(lox\text{-}neo\text{-}lox)}$ knock-in mouse lines were described previously (Pasqualetti et al., 2002). $Wnt1::Cre;Hoxa2^{EGFP(lox\text{-}neo\text{-}lox)/+}$ embryos were obtained by crossing $Hoxa2^{EGFP(lox\text{-}neo\text{-}lox)/+}$ mice with *Wnt1::Cre* mice (Danielian et al., 1998). The following lines were also used: $CMV::CreER^{T2}$ (Santagati et al., 2005), $Hoxa2^{lox}$ (Ren et al., 2002), $Bmp4^{loxP\text{-}lacZ}$ [(Kulessa and Hogan, 2002); hereafter referred to as $Bmp4^{lox}$]. $Hoxa2^{del/+}$ or $Bmp4^{del/+}$ alleles were generated by Cre-mediated deletion, mating *CMV::Cre* (Dupé et al., 1997) with $Hoxa2^{lox/lox}$ or $Bmp4^{lox/lox}$ mice, respectively. To generate $CMV::CreER^{T2};Hoxa2^{lox/del}$ embryos, $Hoxa2^{lox/lox}$ or $Hoxa2^{lox/+}$ were crossed with $CMV::CreER^{T2};Hoxa2^{del/+}$ mice. To generate $Bmp4^{lox/del}$ embryos, $Bmp4^{lox/lox}$ were crossed with $Bmp4^{del/+}$ mice. To generate $Wnt1::Cre^{Hoxa2\text{-}IRES\text{-}EGFP}$ mice, the $Rosa^{(lox\text{-}stop\text{-}lox)Hoxa2\text{-}IRES\text{-}EGFP/+}$ line (Miguez et al., 2012) was crossed with the *Wnt1::Cre* line. All animal experiments were approved by the Basel Cantonal Veterinary Authorities and conducted in accordance with the Guide for Care and Use of Laboratory Animals.

Tamoxifen treatment

Tamoxifen (TM) (Sigma) was dissolved at 20 mg/ml in pre-warmed corn oil (Sigma) and stored at 4°C. Three successive TM administrations (10 mg at E12.5, E13.0 and E13.5) were administered to pregnant females by oral gavage with 12-hour intervals.

Alkaline phosphatase staining

E14.5 mouse fetuses were fixed overnight in 4% paraformaldehyde (PFA), rinsed in PBS, equilibrated in 20% sucrose and embedded in Cryomatrix (Thermo Electron Corporation). Cryostat sections (20 μm) were cut in the frontal and horizontal planes (see Fig. 1A). Sections were fixed for 1 hour in 4% PFA, rinsed in PBS at room temperature and incubated for 1 hour in PBS at 65°C to inactivate endogenous alkaline phosphatase. Sections were rinsed in a solution of NTMT [0.1 M NaCl, 0.1 M Tris-HCl (pH 9.5), 0.05 M $MgCl_2$, 0.1% Tween 20]. For the staining, 3.5 μl NBT (Roche 1383213) and 3.5 μl BCIP (Roche 1383221) were used per ml of NTMT. Sections were rinsed in water, then in 100% ethanol, and mounted onto slides.

Immunohistochemistry

Immunostaining for EGFP on cryosections was performed using a polyclonal rabbit anti-EGFP antibody (Molecular Probes) and a peroxidase-conjugated goat anti-rabbit IgG (Beckman Coulter) or an Alexa 488-conjugated secondary antibody (Invitrogen). For peroxidase-conjugated goat anti-rabbit IgG, detection was performed with DAB chromogen (DAKO). Immunostaining for RFP on cryosections was performed using a polyclonal rabbit anti-RFP antibody (Rockland) and an Alexa 568-conjugated secondary antibody (Invitrogen). Immunostaining for Ki67 was performed on paraffin sections using a rabbit anti-Ki67 antibody (Novocastra NCL-Ki67p) and a biotinylated anti-rabbit antibody. After incubating for 30 minutes at room temperature with the VECTASTAIN ABC reagent (Vector Labs), peroxidase activity was revealed with DAB chromogen. For phosphorylated Smad (phosphoSmad) staining, cryostat sections were incubated with phosphoSmad1/5/8 antibody (Cell Signaling) at 37°C for 3 hours, followed by Alexa 488-conjugated secondary antibody (Invitrogen).

Three-dimensional reconstruction of tissue sections

Consecutive cryostat sections (25 μm) of E14.5 $Hoxa2^{EGFP/+}$ and $Hoxa2^{EGFP/EGFP}$ fetuses, immunostained for EGFP, were imaged with a Leica fluorescence macroscope. Between 49 and 68 sections were aligned using Bitplane AutoAligner 6.0.1 (manual alignment). Structures were artificially labelled in separated channels in Adobe Photoshop CS5.1. The artificially labelled structures, as well as the GFP channel, were transformed into surfaces in Bitplane Imaris 7.5.2 (surface area detail level: 35 μm; thresholding: absolute intensity).

In situ hybridisation

In situ hybridisation on frontal and horizontal sections (see Fig. 1A) were performed as described (Santagati et al., 2005). The following RNA probes were used: *Hoxa2* (Ren et al., 2002), *Eya1* (Xu et al., 1999), *Bmp5* (Solloway and Robertson, 1999), *Bmp4* (Hogan et al., 1994), *Tsg* (Zakin and De Robertis, 2004), *Prrx1*, *Prrx2* (ten Berge et al., 1998) and *Tshz2* (Caubit et al., 2000).

ChIP analysis

ChIP experiments were performed on second pharyngeal arches isolated from E11.5 CD1 embryos as described (Donaldson et al., 2012). Immunoprecipitated DNA was subjected to qPCR using the following primers: *Bmp4*, forward 5′-TGTGGGATAAAACAGGAGTGC-3′ and reverse 5′-GCTCCCTCAGTTTGGCTAGA-3′; *Bmp5*, forward 5′-TATGCAGTCTAGGGCCACCT-3′ and reverse 5′-CATTTGGGATAA-AAGAACCTCAA-3′.

RESULTS

The whole mouse pinna derives from *Hoxa2*$^+$ second arch NCCs

External ear morphogenesis occurs early in development, starting at E12.0 in mouse or at the sixth week in humans. In humans, the auricle was proposed to derive from tubercles, or hillocks, which originate from spatially segregated NCC populations of both first and second pharyngeal arches (reviewed by Hunter and Yotsuyanagi, 2005). To map second arch neural crest contribution to the mouse pinna, we crossed a *rhombomere (R)4::Cre* mouse line (Oury et al., 2006) with the *Z/AP* (Lobe et al., 1999) or *Rosa-CAG-LSL-tdTomato* (Ai14) (Madisen et al., 2010) reporter lines. Upon Cre-mediated recombination, *Alkaline phosphatase* (*AP*) or *tdTomato* gene expression is permanently activated in R4-derived

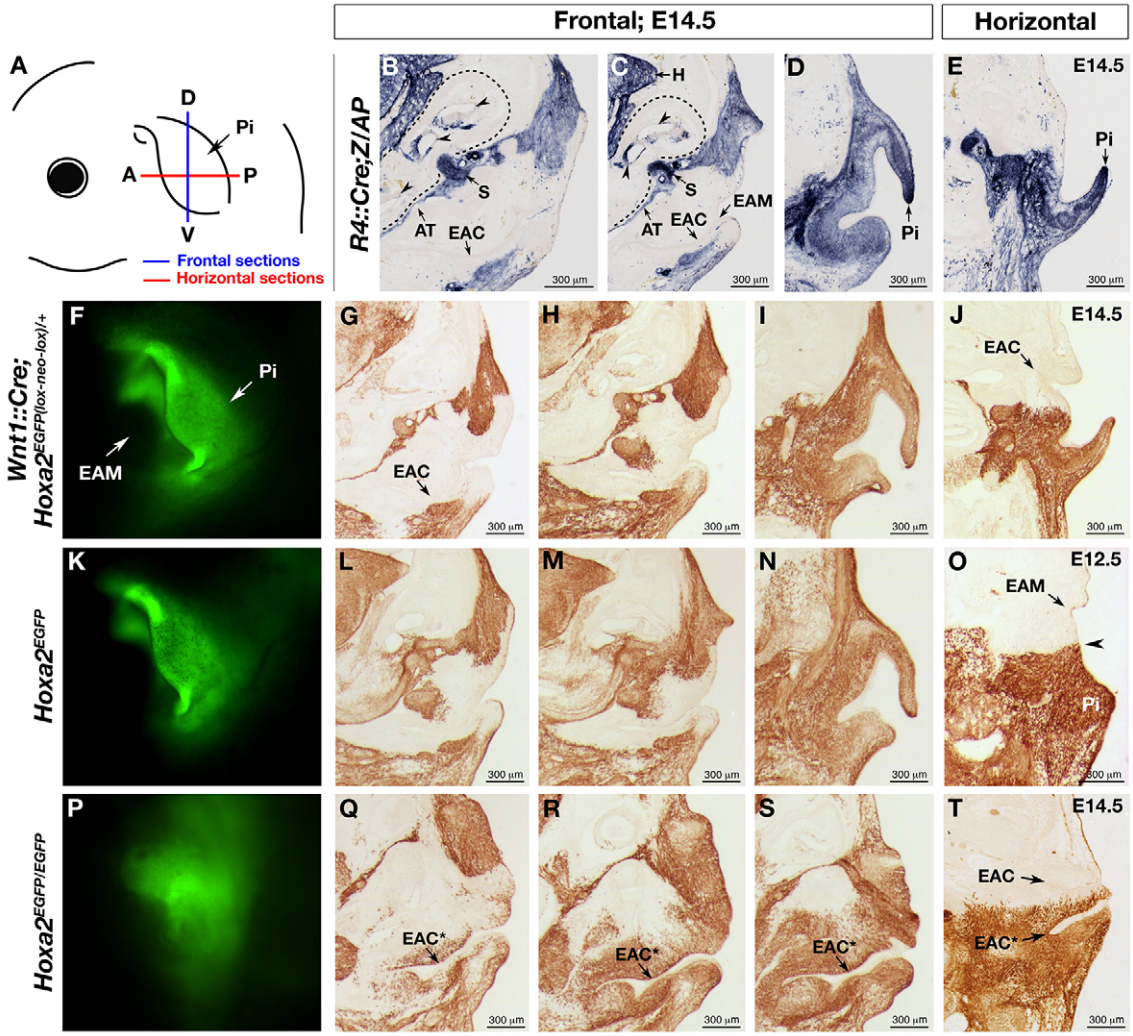

Fig. 1. Fate map of the mouse external ear. (**A**) Drawing representing a lateral view of the head of a newborn mouse. Blue and red lines indicate the frontal and horizontal section planes used in this study. (**B-E**) Z/AP staining performed on frontal (B-D) and horizontal (E) sections through the external ear of E14.5 *R4::Cre;Z/AP* fetuses. (**F**,**K**,**P**) Lateral views under the epifluorescence macroscope of the pinna of E14.5 *Wnt1::Cre;Hoxa2*$^{EGFP(lox\text{-}neo\text{-}lox)/+}$ (F), *Hoxa2*$^{EGFP/+}$ (K) and *Hoxa2*$^{EGFP/EGFP}$ (P) fetuses. (**G-J**,**L-O**,**Q-T**) Anti-EGFP immunostaining on frontal (G-I,L-N,Q-S) and horizontal (J,O,T) sections through the external ear of E12.5 *Hoxa2*$^{EGFP/+}$ (O), E14.5 *Wnt1::Cre;Hoxa2*$^{EGFP(lox\text{-}neo\text{-}lox)/+}$ (G-J), E14.5 *Hoxa2*$^{EGFP/+}$ (L-N) and E14.5 *Hoxa2*$^{EGFP/EGFP}$ (Q-T) fetuses. In B,C,G,H,J,L,M, note that the EAC is lined by EGFP$^-$ cells. In Q-T, note that the duplicated EAC (EAC*) is lined by EGFP$^+$ cells. In O, the arrowhead maps the position of vestigial first pharyngeal cleft at the interface between EGFP$^+$ and EGFP$^-$ territories. In B and C, the otic capsule is outlined and arrowheads indicate the membranous labyrinth. In horizontal sections, top is anterior, bottom is posterior. Frontal sections are from anterior to posterior, top is dorsal, bottom is ventral. A, anterior; AT, auditory tube; D, dorsal; EAM, external auditory meatus; EAC, external auditory canal; H, hindbrain; P, posterior; Pi, pinna; S, stapes; V, ventral.

NCC progenitors, thus allowing second arch NCC contribution to the external ear to be assessed. Although the presence of a few spared unstained cells cannot be ruled out, careful observation of consecutive sections (Fig. 1D,E), as well as high magnifications of co-stainings of tdTomato with DAPI to identify cell nuclei (supplementary material Fig. S1), revealed that the whole mouse pinna is contributed by R4-derived second arch NCCs, and not by a composite of spatially segregated first and second arch NCC-derived mesenchyme.

Hoxa2 is expressed in second, but not in first, arch NCCs (reviewed by Minoux and Rijli, 2010). To map the contribution of *Hoxa2*-expressing (*Hoxa2*$^+$) NCCs to the pinna, we crossed the *Wnt1::Cre* driver (Danielian et al., 1998), which expresses Cre in NCC progenitors, to the *Hoxa2*$^{EGFP(lox\text{-}neo\text{-}lox)}$ allele (Pasqualetti et al., 2002), in which *EGFP* is knocked in at the *Hoxa2* locus and is conditionally induced by Cre-mediated excision. In E14.5 *Wnt1::Cre;Hoxa2*$^{EGFP(lox\text{-}neo\text{-}lox)/+}$ fetuses, the pinna is composed of *EGFP*-expressing NCCs (Fig. 1F,I,J), indicating that this structure mainly originates from *Hoxa2*$^+$ NCC progenitors. Moreover, high magnification of DAPI/EGFP co-stainings (supplementary material Fig. S1) revealed that virtually all cells in the pinna are EGFP$^+$, i.e. they derive from *Hoxa2*$^+$ NCC progenitors. Together with the R4 fate mapping, these results indicate that the mouse pinna mainly originates from *Hoxa2*$^+$ second arch NCCs.

The EAC develops from first arch *Hoxa2*$^-$ ectomesenchyme

In humans, the EAC, an ectodermal structure lined by NCC-derived mesenchyme, has been proposed to originate at the first pharyngeal cleft, i.e. at the interface between the first and second arches, and to

be surrounded by NCCs contributed by both arches (Jakubíková et al., 2005; Schoenwolf and Larsen, 2009). Contrary to this prediction, we found that in E14.5 *Wnt1::Cre;Hoxa2*$^{EGFP(lox\text{-}neo\text{-}lox)/+}$ mouse fetuses the EAC and its surrounding mesenchyme are entirely composed of *Hoxa2*$^{-}$/*EGFP*$^{-}$ cells, and therefore not derived from the second arch (Fig. 1G,H,J). Moreover, we observed a sharp spatial segregation between *Hoxa2*$^{-}$/*EGFP*$^{-}$ and *Hoxa2*$^{+}$/*EGFP*$^{+}$ cell populations contributing to the EAC and the pinna, respectively (Fig. 1J). A similar cell sorting was observed in E14.5 *Hoxa2*$^{EGFP/+}$ fetuses in which *EGFP* is knocked in at the *Hoxa2* locus and faithfully recapitulates the *Hoxa2* expression domain (Pasqualetti et al., 2002) (Fig. 1K-N). Analysis at E12.5 confirmed that mouse EAC begins to form entirely anterior to the second arch-derived *Hoxa2*$^{+}$/*EGFP*$^{+}$ cells that form the pinna, within the *Hoxa2*$^{-}$/*EGFP*$^{-}$ first arch-derived tissue (Fig. 1O). Thus, at E12.5 the EAC and the pinna develop opposite to and almost equidistant from the vestigial first pharyngeal cleft that maps at the border between *EGFP*$^{+}$ and *EGFP*$^{-}$ territories (arrowhead, Fig. 1O); notably, their respective cell contributions from the first and second arches never intermingle despite the complex morphogenetic cell movements that occur during their formation.

To investigate the spatial distribution of second arch cells in the absence of *Hoxa2* function, we used *Hoxa2*$^{EGFP/EGFP}$ homozygous mutant embryos (Fig. 1P). By 3D reconstruction of tissue sections, we confirmed the previously described duplication of the EAC (Gendron-Maguire et al., 1993; Mallo and Gridley, 1996; Mark et al., 1995; Rijli et al., 1993) (EAC*, Fig. 2) and found that the EAC*

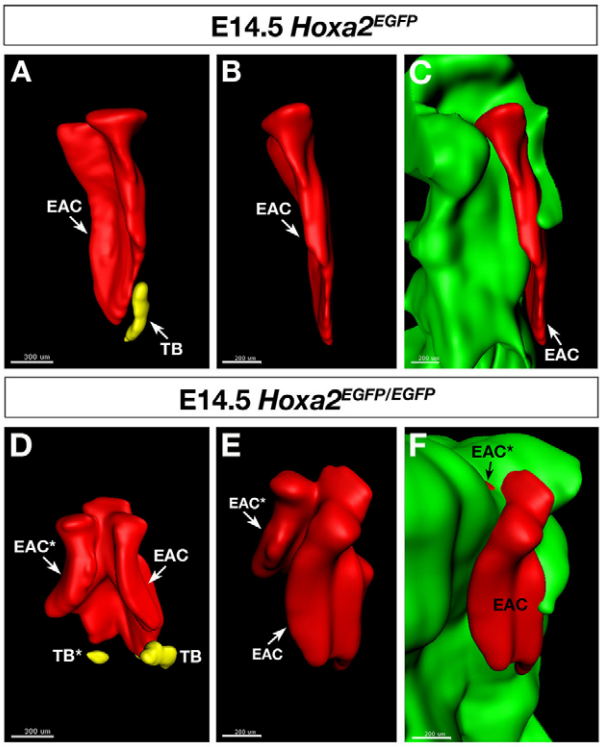

Fig. 2. Three-dimensional reconstruction of the external ear of *Hoxa2*$^{EGFP/+}$ and *Hoxa2*$^{EGFP/EGFP}$ fetuses. (**A-C**) 3D reconstruction of the external auditory canal (EAC; red), tympanic bone (TB; yellow) and EGFP^{+} domain (green) in E14.5 *Hoxa2*$^{EGFP/+}$ control heterozygous fetuses. (**D-F**) 3D reconstruction of the EAC and its duplicated counterpart (EAC*; red), the tympanic bone and its duplicated counterpart (TB*; yellow) and EGFP^{+} domain (green) in E14.5 *Hoxa2*$^{EGFP/EGFP}$ homozygous mutant fetuses.

develops within the *Hoxa2*$^{+}$/*EGFP*$^{+}$ domain (Fig. 2, see also Fig. 1Q-T). By contrast, the orthotopic EAC fully develops into the *Hoxa2*$^{-}$/*EGFP*$^{-}$ territory, both in E14.5 *Hoxa2*$^{EGFP/+}$ control and *Hoxa2*$^{EGFP/EGFP}$ homozygous mutant fetuses (Fig. 2, see also Fig. 1L,M,T). The border between *EGFP*$^{+}$ and *EGFP*$^{-}$ territories appears to be the axis of symmetry, on either side of which the EAC and its ectopic EAC* counterpart develop (Fig. 1T). Tissue sections additionally show that in E14.5 *Hoxa2*$^{EGFP/EGFP}$ homozygous mutant fetuses, the *EGFP*$^{+}$ cells maintain their normal spatial segregation and do not ectopically intermingle with *EGFP*$^{-}$ cells, despite the fact they have acquired a first arch-like identity (Fig. 1T).

Hoxa2 organises spatial patterns of cell proliferation during external ear morphogenesis

At E14.5, *Hoxa2* expression extensively overlaps with the developing pinna. On horizontal and frontal sections, the *Hoxa2*$^{+}$ domain contains an outer territory, which includes the pinna, and an inner territory (Fig. 3B,H, the dashed line delimits the territories). The inner domain is strongly *Hoxa2*$^{+}$, whereas the outer domain displays sparser *Hoxa2* transcript distribution (Fig. 3B,H). The two *Hoxa2*$^{+}$ territories roughly abut at the base of the bending pinna (arrows, Fig. 3B,H). *Hoxa2* is additionally expressed in the mesenchyme at the tip and below the ectoderm on both the dorsal and ventral sides of the pinna (Fig. 3B,H).

The spatial distribution of *Hoxa2* transcripts suggests distinct proliferation/differentiation states of cellular subsets. In E14.5 control fetuses, Ki67^{+} proliferating cells are present at the tip and are orderly aligned on both the dorsal and ventral sides of the pinna, below the ectoderm, whereas the mesenchymal core of the pinna is only contributed by Ki67^{-} postmitotic differentiating cells (Fig. 3A,C,G). At the pinna distal edge (tip), the Ki67^{+} cell pattern overlaps with the *Hoxa2* transcript distribution (Fig. 3A,B), indicating that *Hoxa2* is mainly expressed in proliferating NCCs. By contrast, the inner *Hoxa2* expression domain encompasses both Ki67^{+} and Ki67^{-} cell subsets (Fig. 3A,B,G,H), with Ki67^{+} cells orderly aligned (arrows, Fig. 3A,C,G) and adjacent to Ki67^{-} differentiating mesenchymal cells. In addition, at E14.5 a subset of spatially organised Ki67^{+} proliferating cells at the base and all along the dorsal aspect of the pinna (arrowheads, Fig. 3A,C,G) does not express *Hoxa2* (Fig. 3A,B,G,H). This latter population of highly proliferating cells selectively expresses *Eya1* (Fig. 3G,I), which is essential for pinna development in mice (Xu et al., 1999). Interestingly, at the beginning of pinna morphogenesis (E12.0-12.5), *Eya1* and *Hoxa2* appear to be co-expressed in a subset of second arch-derived NCCs at the base of the future pinna (Fig. 3M-O), which are likely to correspond to the precursors of the *Eya1*$^{+}$ population observed at later stages (Fig. 3I). In E12.5 *Hoxa2* homozygous mutant embryos, this early *Eya1* expression domain is lacking (Fig. 3P,Q).

In control *Hoxa2*$^{lox/del}$ fetuses, which bear both a fully deleted and a floxed *Hoxa2* allele (Ren et al., 2002), the pinna is of normal appearance (Santagati et al., 2005) (Fig. 3A-C), indicating that *Hoxa2* haploinsufficiency in mouse does not result in gross external ear defects. By contrast, tamoxifen (TM) administration to *CMV::CreER*^{T2}*;Hoxa2*$^{lox/del}$ fetuses at NCC postmigratory stages (E12.5, E13.0 and E13.5) induces a hypomorphic pinna (Santagati et al., 2005) (supplementary material Fig. S2), thus bypassing an early role of *Hoxa2* and supporting a late requirement in pinna morphogenesis. The smaller and dysmorphic pinna of TM-treated *CMV::CreER*^{T2}*;Hoxa2*$^{lox/del}$ mutant newborns (supplementary material Fig. S2) is reminiscent of the *HOXA2* mutant phenotype in humans (Alasti et al., 2008). Analysis by *in situ* hybridisation

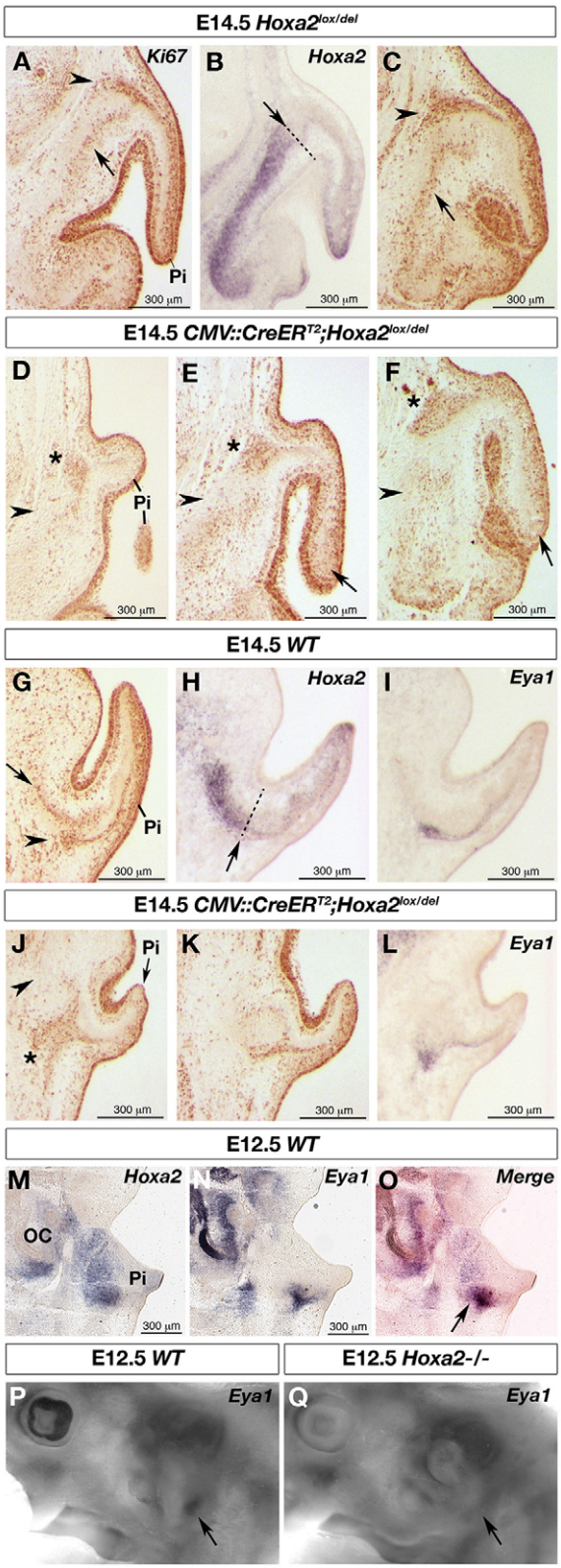

Fig. 3. *Hoxa2* organises spatial patterns of cell proliferation in the pinna. (**A-L**) Anti-Ki67 immunostaining (A,C-G,J,K) and *Hoxa2* (B,H) and *Eya1* (I,L) *in situ* hybridisation on frontal (A-F) and horizontal (G-L) sections through the external ear of E14.5 *Hoxa2*$^{lox/del}$ control (A-C), wild-type (WT) (G-I) and *CMV::CreER*^{T2}*;Hoxa2*$^{lox/del}$ (D-F,J-L) tamoxifen (TM)-treated fetuses at E12.5, E13.0 and E13.5. Frontal sections are from anterior to posterior, top is dorsal, bottom is ventral. In horizontal sections, top is anterior, bottom is posterior. In B and H, the dashed line separates outer from inner *Hoxa2*$^{+}$ territories, abutting at the base of the bending pinna (arrows). In A,C,G, arrows indicate orderly aligned proliferating cells in the inner *Hoxa2*$^{+}$ domain; arrowheads indicate orderly aligned proliferating cells at the base of the pinna and extending along its dorsal aspect. In D-F,J, arrows and arrowheads indicate altered spatial segregation of Ki67^{+} and Ki67^{-} mesenchymal cells in the pinna (E,F) and in the inner domain (D-F,J), respectively. Asterisks indicate an unpatterned mass of proliferating cells accumulating at the dorsal base of the pinna. (**M-O**) *In situ* hybridisation on adjacent horizontal sections through the external ear of E12.5 wild-type embryo using *Hoxa2* (M) and *Eya1* (N) probes. In O, the images in M and N have been merged to highlight *Hoxa2* and *Eya1* co-expression in a subset of second arch NCCs (arrow). Top is anterior, bottom is posterior. (**P**,**Q**) *Eya1* whole-mount *in situ* hybridisation on E12.5 wild-type (P) and *Hoxa2* homozygous mutant (Q) embryos. OC, otic capsule; Pi, pinna.

confirmed the almost complete loss of *Hoxa2* expression in TM-treated mutants when compared with control embryos (supplementary material Fig. S3).

At E14.5, no apoptotic cells were observed in control or in TM-treated *CMV::CreER*^{T2}*;Hoxa2*$^{lox/del}$ mutant fetuses (not shown), suggesting that the smaller dysmorphic pinna is not the result of increased cell death. This was also indirectly supported by the persistence of *EGFP*$^{+}$ cells in the outer ear region of *Hoxa2*$^{EGFP/EGFP}$ full knockout fetuses, which lack a normal pinna (Fig. 1P-T). The hypomorphic pinna of E14.5 TM-treated *CMV-CreER*^{T2}*;Hoxa2*$^{lox/del}$ fetuses lacks the normal spatial segregation between Ki67^{+} and Ki67^{-} mesenchymal cells (arrows, Fig. 3E,F). Moreover, a mass of proliferating cells abnormally accumulates at the dorsal base of the pinna (asterisks, Fig. 3D-F,J), and the inner *Hoxa2*$^{+}$ domain appears disorganised, with fewer Ki67^{+} cells and an accumulation of unpatterned Ki67^{-} differentiating cells (arrowheads, Fig. 3D-F,J). Lastly, in E14.5 TM-treated *CMV-CreER*^{T2}*;Hoxa2*$^{lox/del}$ fetuses, the population of spatially organised proliferating cells that expresses *Eya1* is still present (Fig. 3L), suggesting a role of *Hoxa2* in establishing, but not maintaining, the proliferative *Eya1*$^{+}$ territory.

Altogether, these results indicate that, after E12.5, *Hoxa2* contributes to the normal size and shape of the pinna by organising spatially restricted local patterns of cell proliferation.

Hoxa2 regulates *Bmp5* and *Bmp4* expression in the developing pinna

The hypomorphic pinna in TM-treated *CMV::CreER*^{T2}*;Hoxa2*$^{lox/del}$ fetuses is reminiscent of the phenotype of the *short ear* mutation, which inactivates *Bmp5* (King et al., 1994; Kingsley et al., 1992). Thus, *Bmp5* is a suitable candidate to be regulated by Hoxa2. In E14.5 control pinna, *Bmp5* expression is restricted to the mesenchymal cores of the inner and outer *Hoxa2*$^{+}$ domains, although not at the tip or in most of the proliferating mesenchyme of the pinna (Fig. 4A,B,E,F). In TM-treated *CMV::CreER*^{T2}*;Hoxa2*$^{lox/del}$ fetuses, *Bmp5* expression levels were strongly reduced in the pinna (arrowheads, Fig. 4M,N). We also observed a reduction in the spatial extent of *Bmp5* expression in the inner *Hoxa2*$^{+}$ domain (arrows, Fig. 4M,N), with an accumulation of *Bmp5* residual expression at the base of the pinna (asterisk, Fig. 4M). *Hoxa2* temporal inactivation selectively downregulates *Bmp5*, although not paired related homeobox 1 (*Prrx1*), which encodes a transcription factor involved in craniofacial development (Martin et al., 1995) (Fig. 4I,J,Q,R).

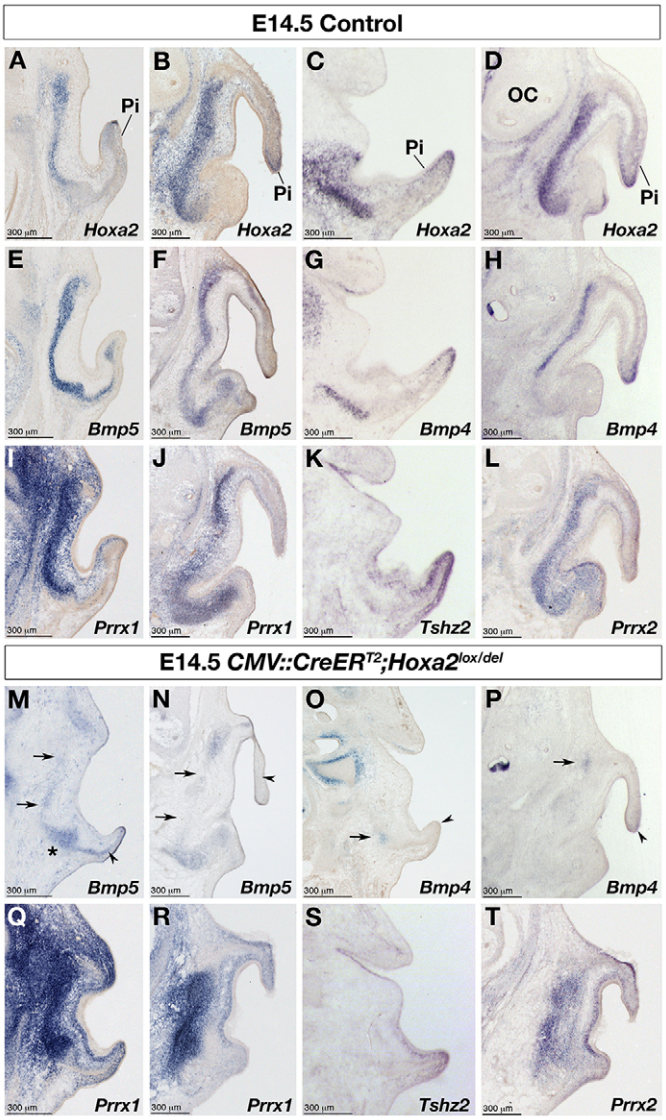

Fig. 4. Hoxa2 positively regulates *Bmp5* and *Bmp4* expression. (**A-T**) *In situ* hybridisation on horizontal (A,C,E,G,I,K,M,O,Q,S) and frontal (B,D,F,H,J,L,N,P,R,T) sections through the external ear of E14.5 control (A-L) and *CMV::CreER^{T2};Hoxa2$^{lox/del}$* mutant fetuses treated with tamoxifen (TM) at E12.5, E13.0 and E13.5 (M-T), using *Hoxa2* (A-D), *Bmp5* (E,F,M,N), *Bmp4* (G,H,O,P), *Prrx1* (I,J,Q,R), *Tshz2* (K,S) and *Prrx2* (L,T) probes. In M-P, arrowheads indicate the reduction of *Bmp5* and *Bmp4* expression levels in the pinna, arrows indicate the reduction in the spatial extent of *Bmp5* (M,N) and *Bmp4* (O,P) expression in the inner *Hoxa2*$^+$ domain, and the asterisk indicates the accumulation of *Bmp5* residual expression at the base of the pinna (M) in TM-treated mutants. Note that the section in D is the same as that in Fig. 3D, and is adjacent to H. In frontal sections, top is dorsal and bottom is ventral. In horizontal sections, top is anterior and bottom is posterior. OC, otic capsule; Pi, pinna.

We next analysed *Bmp4* expression. At E12.0-12.5, *Bmp4* is expressed at the distal edge (tip) of the forming pinna, as well as in a small population of mesenchymal cells at its base (not shown). This pattern is maintained and extended at E13.5 and E14.5, becoming similar to the *Hoxa2* expression pattern. Specifically, *Bmp4* is highly expressed in the mesenchymal core of the inner *Hoxa2*$^+$ domain (Fig. 4C,D,G,H). In the pinna, *Bmp4* is expressed at the tip and in the proliferating mesenchyme below the dorsal and ventral ectoderm (Fig. 4G,H). This transcript distribution is complementary to that of *Bmp5* (supplementary material Fig. S4A,B); notably, the *Bmp4* and *Bmp5* expression patterns together recapitulate the *Hoxa2* expression pattern in the pinna (Fig. 4A-H). In E14.5 TM-treated *CMV::CreER^{T2};Hoxa2$^{lox/del}$* mutant pinna, *Bmp4* expression is absent or strongly reduced (Fig. 4O,P), whereas *Prrx1* (Fig. 4J), *Prrx2* (Fig. 4L) (ten Berge et al., 1998) and teashirt zinc finger family member 2 (*Tshz2*) (Caubit et al., 2000) (Fig. 4K) are still expressed in the inner *Hoxa2*$^+$ domain and at the tip of the pinna (Fig. 4S,T; data not shown).

In summary, the above results indicate that *Hoxa2* is required to maintain the normal levels and spatial distribution of *Bmp4* and *Bmp5* transcripts during pinna growth and morphogenesis.

Temporal inactivation of *Hoxa2* results in altered BMP signalling in the developing pinna

The activity of BMPs is modulated in the extracellular space through their interaction with secreted agonists or antagonists. Tsg is a secreted BMP modulator involved in mouse head development (Zakin and De Robertis, 2004). Although no external ear defects are observed in *Tsg*$^{-/-}$ or *Bmp4*$^{+/-}$ mice, compound *Tsg*$^{-/-}$;*Bmp4*$^{+/-}$ newborns display, in severe cases, low-set ears associated with an abnormal shape of the pinna (Zakin and De Robertis, 2004), indicating that Tsg is involved in modulating Bmp4 activity during pinna development. In E14.5 wild-type fetuses, *Tsg* is strongly expressed in a stripe of Ki67$^+$ highly proliferating cells in the inner *Hoxa2*$^+$ domain (supplementary material Fig. S5K, arrow; Fig. 3G, arrow), directly adjacent to the *Bmp4*$^+$ mesenchymal core (supplementary material Fig. S5A-O). In E14.5 TM-treated *CMV::CreER^{T2};Hoxa2$^{lox/del}$* pinna, *Tsg* is severely downregulated (supplementary material Fig. S5P-R). These results, together with the downregulation of *Bmp4* and *Bmp5* expression and the effects on cell proliferation patterns (Figs 3, 4), further support the notion that *Hoxa2* is involved in BMP signalling regulation during pinna formation.

To further investigate the downstream effects induced by *Bmp5*, *Bmp4* and *Tsg* downregulation in *Hoxa2* mutants, we analysed the phosphorylation of Smad1, 5 and 8, a hallmark of canonical BMP signal transduction (Heldin and Moustakas, 2012; Horbelt et al., 2012), by anti-phosphoSmad1/5/8 immunostaining. In E14.5 control fetuses, the phosphoSmad1/5/8$^+$ cell distribution is spatially restricted. PhosphoSmad1/5/8$^+$ cells are observed throughout the *Bmp5*$^+$/*Bmp4*$^+$ territory of the inner *Hoxa2*$^+$ domain extending to the base of the pinna (white arrows, Fig. 5A,C; supplementary material Fig. S4C), although not in the *Bmp5*$^+$/*Bmp4*$^-$ mesenchymal core of the developing pinna (Fig. 5A,C; supplementary material Fig. S4A-C). PhosphoSmad1/5/8$^+$ cells are also detected in the *Ki67*$^+$/*Bmp4*$^+$ proliferating domain at the tip of the pinna (green arrowheads, Fig. 5A,C; supplementary material Fig. S4A,C), and in the *Eya1*$^+$/*Ki67*$^+$ highly proliferative domain abutting the pinna mesenchymal core (white arrowheads, Fig. 5A,C; supplementary material Fig. S4C).

In E14.5 TM-treated *CMV::CreER^{T2};Hoxa2$^{lox/del}$* pinna, co-staining between phosphoSmad1/5/8 antibody and DAPI shows that phosphoSmad1/5/8$^+$ domains at the base and at the tip of the pinna are either strongly reduced or absent (white arrows and green arrowheads, Fig. 5E-H). These data indicate that *Hoxa2* temporal inactivation has strong effects on the local regulation of canonical BMP signalling. By contrast, the *Eya1*$^+$ subpopulation of phosphoSmad1/5/8$^+$ cells is still present (white arrowheads, Fig. 5E,G), in keeping with the observation that the late *Hoxa2* inactivation only partially affects this *Eya1*$^+$ cell population (see above; Fig. 3I,L).

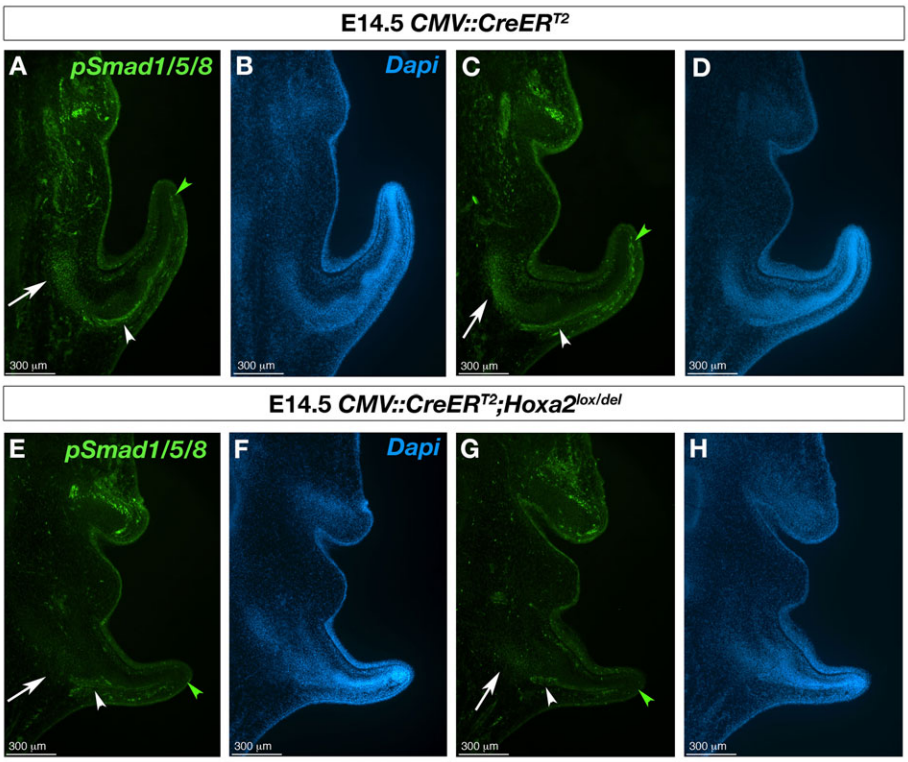

Fig. 5. *Hoxa2* temporal inactivation affects the BMP signalling pathway. (**A-H**) Anti-phosphoSmad1/5/8 immunostaining (A,C,E,G) and DAPI staining (B,D,F,H) of horizontal sections through the external ear of E14.5 *CMV::CreER*^{T2} control (A-D) and *CMV::CreER*^{T2}*;Hoxa2*$^{lox/del}$ mutant (E-H) fetuses treated with tamoxifen (TM) at E12.5, E13.0 and E13.5. A and B, C and D, E and F, G and H are the same sections co-stained for both anti-phosphoSmad1/5/8 and DAPI. In E,G, phosphoSmad1/5/8 staining is absent or strongly reduced at the tip of the pinna (green arrowheads) and in the inner *Hoxa2*$^{+}$ domain (white arrows), but is maintained in the *Eya1*$^{+}$ subpopulation abutting the pinna mesenchymal core (white arrowheads). Top is anterior, bottom is posterior.

Role of *Bmp4* in external ear morphogenesis

Bmp4$^{lox/+}$ (Kulessa and Hogan, 2002) heterozygous mutant mice survive and do not show external ear defects (not shown). To investigate the consequences of further reducing *Bmp4* activity during pinna morphogenesis, we generated *Bmp4*$^{lox/del}$ hypomorphic mutants bearing both a fully deleted and a floxed *Bmp4* allele. Unlike null mutants, *Bmp4*$^{lox/del}$ fetuses survive until E16.5, a stage at which the pinna has normally already folded over the meatus (Fig. 6A,D). In severe cases, *Bmp4*$^{lox/del}$ fetuses display a hypomorphic pinna (Fig. 6B,F), albeit at low frequency (n=5/22). When present, this phenotype is always associated with polydactyly (arrows, Fig. 6E, compare with 6C), which also occurs at a low frequency (n=9/22) in these hypomorphic mutants. Bilateral microphthalmia, smaller body size and subcutaneous edema are also observed in most of the *Bmp4*$^{lox/del}$ hypomorphic mutants (Fig. 6A,B). The weak penetrance of the pinna phenotype is likely to be due to partial functional redundancy with other BMP family members, such as *Bmp5*, and/or the persistence of residual *Bmp4* function in *Bmp4*$^{lox/del}$ hypomorphic mutants. *Bmp4* homozygous null mutants die around gastrulation (Winnier et al., 1995), preventing analysis of its role in external ear morphogenesis. Nonetheless, these results highlight *Bmp4* involvement, at least to some extent, in the morphogenesis of the pinna.

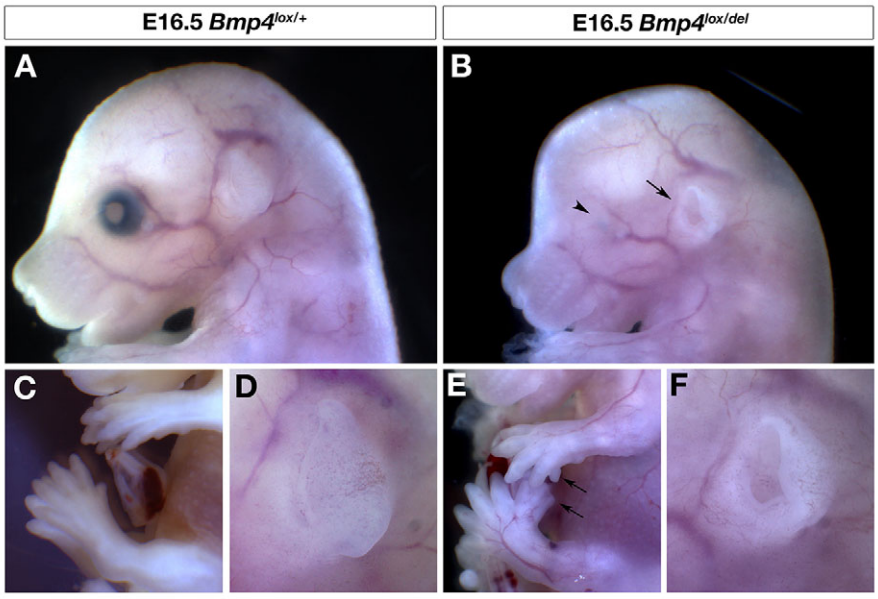

Fig. 6. *Bmp4* involvement in pinna morphogenesis. Lateral views of E16.5 (**A**,**C**,**D**) *Bmp4*$^{lox/+}$ control and (**B**,**E**,**F**) *Bmp4*$^{lox/del}$ hypomorphic mutant fetuses. (C,D) Enlarged views of the hindlimb and pinna of the fetus in A. In B, the arrowhead indicates the apparent lack of normal eyes, and the arrow points to a small pinna, which is magnified in F. In E, the arrows indicate polydactyly.

Hoxa2 binds to *Bmp4* and *Bmp5* non-coding regions in second pharyngeal arch

By mining datasets from a genome-wide map of Hoxa2 binding to chromatin (ChIP-Seq) from second pharyngeal arch tissue dissected just prior to external ear formation (Donaldson et al., 2012), we found binding of Hoxa2 in proximity to *Bmp4* [72 kb downstream of the *Bmp4* transcription start site (TSS)] and within the third intron of *Bmp5* (52 kb upstream of the *Bmp5* TSS). We confirmed Hoxa2 binding enrichment on both *Bmp4* and *Bmp5* regions by performing conventional ChIP on second arches dissected from E11.5 wild-type embryos (supplementary material Fig. S6A). The region bound by Hoxa2 in the third intron of *Bmp5* is the result of an insertion that is present only in mice and rat. By contrast, the region located downstream of the *Bmp4* TSS is widely conserved in vertebrates and contains putative Pbx/Hox and Hox binding sites (supplementary material Fig. S6B). Moreover, in E11.5 *Hoxa2* mutant second arch the expression of both *Bmp4* and *Bmp5* is downregulated (Donaldson et al., 2012). Together with the expression pattern changes observed in temporally induced *Hoxa2* mutants (Fig. 4), these results suggest that Hoxa2 might directly maintain *Bmp4* and *Bmp5* expression in spatially restricted domains of the developing external ear.

Hoxa2 is sufficient to induce an ectopic pinna

To address whether *Hoxa2* is not only necessary but also sufficient for the formation of the pinna we established a conditional overexpression system in the mouse allowing ectopic *Hoxa2* expression in Hox-negative NCCs anterior to the second arch. Conditional *Hoxa2* overexpression in NCCs was induced by mating the *Wnt1::Cre* line (Danielian et al., 1998) with a $Rosa^{(lox\text{-}stop\text{-}lox)Hoxa2\text{-}IRES\text{-}EGFP}$ allele (Miguez et al., 2012) to produce $Wnt1::Cre;Rosa^{(lox\text{-}stop\text{-}lox)Hoxa2\text{-}IRES\text{-}EGFP}$ (hereafter designated $Wnt1^{Hoxa2\text{-}IRES\text{-}EGFP}$).

$Wnt1^{Hoxa2\text{-}IRES\text{-}EGFP}$ fetuses die at birth and display craniofacial defects, including face, middle ear and skull bone malformations, as well as a reduction in lower jaw size (Fig. 7; data not shown). Most notably, all of them (n=25/25) display an ectopic, fully formed pinna, which is a mirror-image duplication of its normal orthotopic counterpart (compare Fig. 7A with supplementary material Fig. S7B-E). The ectopic pinna replaces the EAC, and thus is likely to form from first arch NCCs. The orthotopic pinna, which is derived from the second pharyngeal arch, appears normally shaped, indicating that *Hoxa2* overexpression from the $Rosa^{(lox\text{-}stop\text{-}lox)Hoxa2\text{-}IRES\text{-}EGFP}$ allele within its own expression domain does not result in overt pinna morphological abnormalities (Fig. 7B-E). It is also noteworthy that $Wnt1^{Hoxa2\text{-}IRES\text{-}EGFP}$ fetuses occasionally display multiple additional ectopic structures around the eye that morphologically resemble small ectopic pinnae (arrows, Fig. 7C,D).

The presence of an internal ribosome entry site (IRES) in the $Rosa^{(lox\text{-}stop\text{-}lox)Hoxa2\text{-}IRES\text{-}EGFP}$ allele allows the cells that are ectopically expressing *Hoxa2* to be traced by immunohistochemistry with an anti-EGFP antibody. We therefore compared the $EGFP^+$ cell distribution in E14.5 $Wnt1::Cre;Hoxa2^{EGFP(lox\text{-}neo\text{-}lox)/+}$ fetuses, in which *EGFP* is conditionally expressed in NCCs expressing the endogenous *Hoxa2* (Fig. 8A), with $Wnt1^{Hoxa2\text{-}IRES\text{-}EGFP}$ fetuses, which additionally ectopically express *Hoxa2-IRES-EGFP* in rostral *Hoxa2*-negative territories. In $Wnt1^{Hoxa2\text{-}IRES\text{-}EGFP}$ mutants, the ectopic pinna is entirely contributed by *Hoxa2-IRES-EGFP*-expressing cells (Fig. 8B-D).

Moreover, the ectopic pinna of $Wnt1^{Hoxa2\text{-}IRES\text{-}EGFP}$ fetuses displays mirror-image duplications of the *Bmp5*, *Bmp4* and *Tsg* expression patterns (Fig. 8E-L; supplementary material Fig. S7). Namely, *Bmp4* is expressed at the tip of the duplicated pinna as well as in the mesenchyme at its base (Fig. 8I-L). *Bmp5* and *Tsg* are expressed in the mesenchymal core and at the base of the duplicated pinna (Fig. 8E-H; supplementary material Fig. S7). Notably, *Bmp4* is also expressed in the ectopic structures that form around the eye (Fig. 8L), while *Bmp5* is expressed in the underlying mesenchyme (Fig. 8F-H). Strikingly, proliferating $Ki67^+$ and differentiating $DAPI^+$ cell patterns are spatially organised in the ectopic pinna as a faithful mirror image of the cellular organisation of the orthotopic pinna (Fig. 8M-Q).

These results not only confirm the molecular identity of the duplicated pinna but also demonstrate that *Hoxa2* is sufficient to

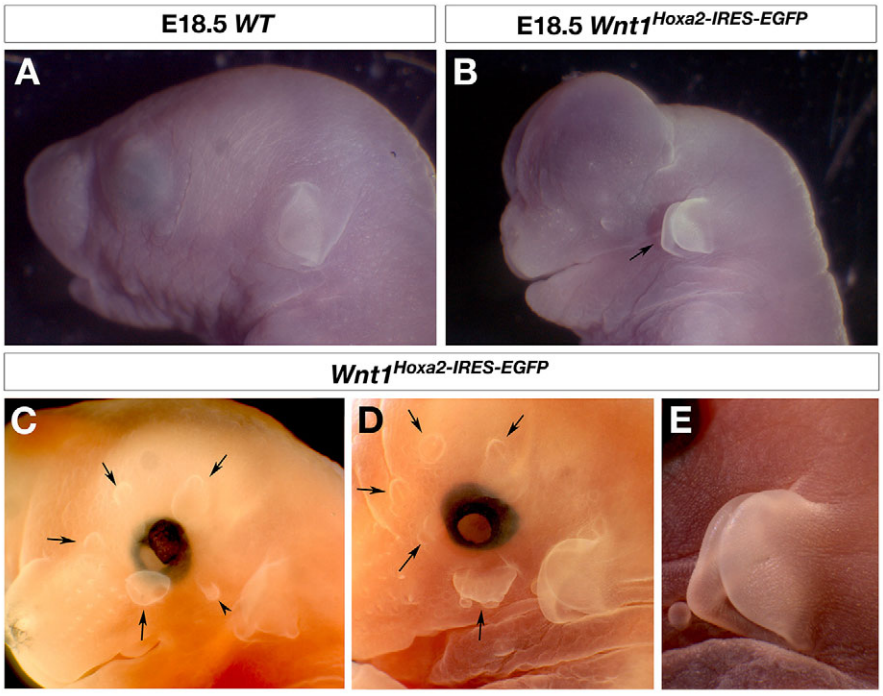

Fig. 7. Hoxa2 expression is sufficient to induce an ectopic pinna. (**A-E**) Lateral views of the head of E18.5 (A,B,E) and E17.5 (C,D) wild-type (A) and $Wnt1^{Hoxa2\text{-}IRES\text{-}EGFP}$ mutant (B-E) fetuses. The arrow in B indicates a duplicated pinna, which is enlarged in E. Arrows in C and D indicate ectopic structures forming all around the eye that resemble small ectopic pinnae.

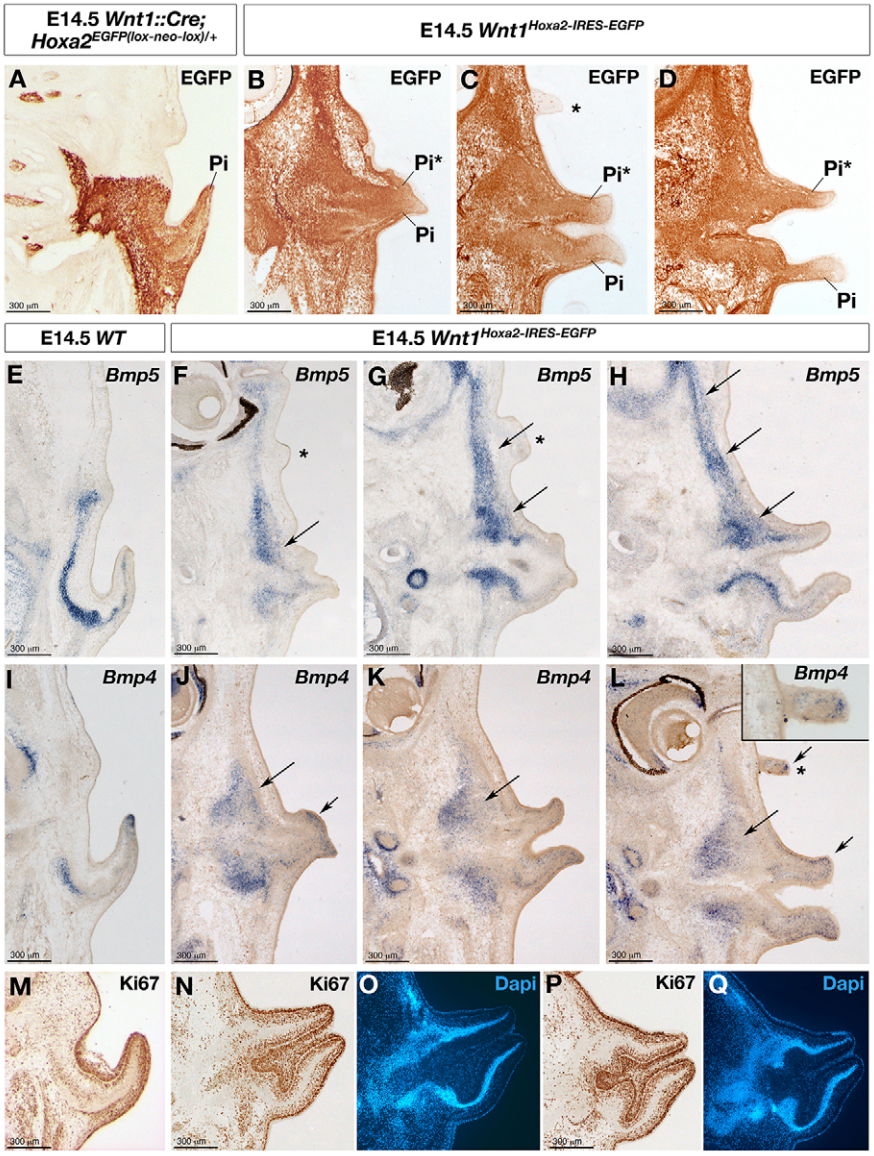

Fig. 8. Molecular identity of Hoxa2-induced pinna. (**A-D**) Anti-EGFP immunostaining on horizontal sections through the external ear of E14.5 *Wnt1::Cre;Hoxa2*$^{EGFP(lox\text{-}neo\text{-}lox)/+}$ control (A) and *Wnt1*$^{Hoxa2\text{-}IRES\text{-}EGFP}$ mutant (B-D) fetuses. (**E-L**) *Bmp5* (E-H) and *Bmp4* (I-L) *in situ* hybridisation on horizontal sections through the external ear of E14.5 wild-type (E,I) and *Wnt1*$^{Hoxa2\text{-}IRES\text{-}EGFP}$ mutant (F-H,J-L) fetuses. Arrows indicate *Bmp5* and *Bmp4* ectopic expression in the duplicated pinna (Pi*) and more anteriorly. Asterisks indicate the ectopic structures that form around the eye, one of which is enlarged in the inset in L. *Bmp4* is expressed in the ectopic structures, whereas *Bmp5* is expressed in the mesenchyme just beneath. (**M-Q**) Anti-Ki67 immunostaining (M,N,P) and DAPI staining (O,Q) on horizontal sections through the external ear of E14.5 wild-type (M) and *Wnt1*$^{Hoxa2\text{-}IRES\text{-}EGFP}$ mutant (N-Q) fetuses. Top is anterior, bottom is posterior. Pi, pinna.

induce and maintain the genetic programme that underlies the formation of the pinna.

DISCUSSION

Revisiting the embryological origin of the external ear

The human auricle cartilage has classically been proposed to derive from six nodular masses of mesenchyme, termed the hillocks of His, that appear during the sixth week of development, three in the first (mandibular) and three in the second (hyoid) pharyngeal arch, respectively (reviewed by Hunter and Yotsuyanagi, 2005; Schoenwolf and Larsen, 2009). On the other hand, the ectodermal EAC has been proposed to originate at the first pharyngeal cleft and to be lined by NCCs contributed by both first and second arches (Jakubíková et al., 2005; Schoenwolf and Larsen, 2009). The hillocks eventually fuse to form the different parts of the human external ear. Although there is consensus that the tragus, projecting in front of the EAC, derives from mandibular hillocks, the respective contributions of mandibular or hyoid hillocks to the auricle are less clear (Hunter and Yotsuyanagi, 2005; Kagurasho et al., 2012). For instance, according to some authors, but not others, first arch-derived hillocks not only form the tragus but also give rise to the helix, which is the auricle folded edge, and the antihelix (reviewed by Hunter and Yotsuyanagi, 2005).

Our genetic fate mapping in the mouse provides novel insights into the embryological origin of the external ear. We show that the mesenchyme just anterior to the EAC (possibly, the mouse homologue of the human tragus) is contributed by *Hoxa2*$^{-}$/*EGFP*$^{-}$ cells (Fig. 1), indicating that, as proposed in humans, it might originate from first pharyngeal arch NCCs. By contrast, genetic fate mapping and *Hoxa2* functional analysis reveal for the first time that the mouse pinna is entirely contributed by second arch *Hoxa2*$^{+}$ neural crest-derived mesenchyme, and not by both first and second arch NCCs. Moreover, genetic fate mapping shows that the ectoderm-derived EAC invaginates into, and is entirely surrounded by, *Hoxa2*-negative mesenchyme, which is both anterior and spatially segregated from second arch-derived mesenchyme (Fig. 1), and is thus most likely of first arch origin. Therefore, the mouse EAC appears to be a first arch-derived structure that does not originate at the border between first arch *Hoxa2*-negative and second arch *Hoxa2*-positive mesenchyme, i.e. at the first pharyngeal cleft, as previously assumed (Jakubíková et al., 2005; Schoenwolf and Larsen, 2009).

Auricle morphology is complex in humans, suggesting that additional components might have been recruited from the developing first arch mesenchyme, as compared with mouse. Nonetheless, it is possible that, as in mouse, the human auricle is mostly contributed by second arch NCCs. This conclusion may be indirectly supported by the following arguments. First, there is agreement among clinicians that the trigeminal (first arch) nerve supply is limited to the tragus and anterior part of the EAC (reviewed by Hunter and Yotsuyanagi, 2005; Wood-Jones and I-Chuan, 1934). Second, the auricle is not affected in otocephaly, which is a genetic syndrome resulting from failure of first arch development. Interestingly, only the tragus, which is known to derive from the first arch, is absent in this syndrome (Hunter and Yotsuyanagi, 2005; Wood-Jones and I-Chuan, 1934). Lastly, based on the analysis of the recurrent localisation in the neighbourhood of the tragus of frequent human congenital abnormalities such as pre-auricular fistulae and appendages, Wood-Jones and I-Chuan (Wood-Jones and I-Chuan, 1934) already came to the conclusion that the human pinna is mainly of hyoid origin. This latter conclusion is now fully supported by our current fate mapping in the mouse, supporting evolutionary conservation of the pharyngeal arch contribution to the definitive external ear in mammals. Overall, our results could be of interest from a clinical standpoint because they might facilitate our understanding of human syndromes, notably concerning the correlation between the embryological origin of the external ear, gene expression patterns, and the interpretation of the phenotypic outcome of their disruption.

Revisiting the EAC phenotype of the *Hoxa2* mutant mouse

By reconsidering the embryological origin of the EAC, our fate map as well as 3D tissue reconstruction allow a better understanding of the previously described mouse *Hoxa2* knockout phenotype (Rijli et al., 1993). The finding that the mouse EAC and its surrounding mesenchyme derive from the first pharyngeal arch and do not develop at the first pharyngeal cleft better explains the observed partial duplication of the EAC in *Hoxa2* mutants (Rijli et al., 1993). Our analysis indicates that, rather than forming the EAC, the first pharyngeal cleft maps at the border between $EGFP^{+}$ and $EGFP^{-}$ NCCs and could represent the axis of symmetry on either side of which a mirror-image duplication of the EAC occurs in *Hoxa2* mutant mice.

Hoxa2 is a major determinant of pinna formation

Hoxa2 inactivation in the mouse results in a mirror-image homeotic transformation of the second arch-derived stapes, styloid process of the temporal bone and lesser horn of the hyoid bone into a duplicated set of first arch-like structures, namely the proximal part of the jaw (Meckel's) cartilage, the incus, malleus, tympanic bone and proximal gonial bone (Gendron-Maguire et al., 1993; Rijli et al., 1993). These structures are normally derived from the Hox-negative NCCs arising from the rostral hindbrain (Köntges and Lumsden, 1996; Kuratani, 2005; Minoux and Rijli, 2010; Rijli et al., 1993; Santagati and Rijli, 2003; Takechi and Kuratani, 2010). This subset of first arch NCCs and second arch NCCs share a common Hox-free ground (default) patterning molecular programme upon which *Hoxa2* expression selects second arch identity (Köntges and Lumsden, 1996; Kuratani, 2005; Minoux et al., 2009; Minoux and Rijli, 2010; Rijli et al., 1993; Santagati and Rijli, 2003; Takechi and Kuratani, 2010). However, the possible extension of this model to other NCC-derived structures, such as the external ear, was not previously assessed.

In $Wnt1^{Hoxa2\text{-}IRES\text{-}EGFP}$ embryos, ectopic *Hoxa2* expression in Hox-negative cranial NCCs induces abnormalities in structures derived from midbrain and forebrain Hox-negative NCCs, such as most of the jaw, facial and skull bones, supporting the notion that ectopic Hox gene expression interferes with normal craniofacial development (e.g. Couly et al., 1998). However, we found that conditional ectopic *Hoxa2* expression is also sufficient to repattern mandibular arch mesenchyme, derived from rostral hindbrain NCCs, and to generate a mirror-image transformation into a second arch-like structure, the pinna, at the expense of the EAC. This further extends the proposal of a Hox-free ground patterning programme shared by hindbrain NCCs, and suggests that the first arch-derived mesenchyme normally lining the EAC has been homeotically transformed into a duplicated pinna, normally a second arch derivative. Lastly, the ability of *Hoxa2* to repattern (a subset of) first arch NCCs appears to be conserved (Grammatopoulos et al., 2000; Pasqualetti et al., 2000). In this respect, we additionally observed in $Wnt1^{Hoxa2\text{-}IRES\text{-}EGFP}$ newborns skeletal morphological changes that could be interpreted as partial transformations of middle ear first arch skeletal elements into second arch-like structures (not shown).

Several cases in the literature have reported partial or total duplication of the human pinna (Baschek et al., 2006; Gore et al., 2006; Hunter and Yotsuyanagi, 2005; Ku et al., 1998; Mishra and Misra, 1978; Pan et al., 2010). Although the genetic basis of such a phenotype has not been investigated, it is tempting to speculate that ectopic HOXA2 expression might underlie the 'polyotia' or 'mirror ear' phenotype observed in humans. As *Hoxa2* alone is able to induce the whole developmental programme underlying the morphogenesis of the pinna, our data moreover suggest that numerous genes involved in human auricle abnormalities are *HOXA2* targets.

Towards an understanding of the molecular mechanisms involved in pinna morphogenesis

Our study provides novel insights into the largely unknown molecular programme involved in external ear morphogenesis. The identification of such a programme could improve our understanding of the *HOXA2* mutant phenotype in humans. Indeed, we have shown that *Hoxa2* regulates the expression of *Eya1*, which is involved in the branchio-oto-renal syndrome in humans (Abdelhak et al., 1997; Kochhar et al., 2007). Our functional and molecular analyses also reveal that *Hoxa2* is involved in the regulation of *Bmp5*, *Bmp4* and *Tsg* expression and Smad1/5/8 activity. Thus, *Hoxa2* acts upstream of the BMP canonical signalling pathway during external ear morphogenesis. A recent study has reported a role for *Hoxa2* in activating the Wnt-β-catenin signalling pathway in the second arch (Donaldson et al., 2012), in part through the regulation of *Wnt5a* expression, a gene that when inactivated in mouse affects external ear development (Qian et al., 2007). Altogether, these data uncover roles for BMP and Wnt signalling in instructing external ear morphogenesis downstream of *Hoxa2*; how these pathways interact remains to be determined. More generally, understanding how multiple genes integrate into functional networks is becoming key to a full comprehension of the molecular processes that underlie normal and defective external ear morphogenesis.

Acknowledgements

We thank F. Santagati and A. Vitobello for experimental assistance and discussion; B. Hogan for the kind gift of the *Bmp4* conditional allele; and L. Fasano for the *Tshz2* probe.

Funding

M.M. was supported by the Faculté de Chirurgie Dentaire de Strasbourg. S.A. was supported by a grant of the Biotechnology and Biological Sciences

Research Council [BB/H018123/2] to N.B. Work in the F.M.R. laboratory is supported by the Swiss National Science Foundation [Sinergia CRSI33_127440], Fondation pour l'Aide à la Recherche sur la Sclérose en Plaques (ARSEP) and the Novartis Research Foundation.

Competing interests statement
The authors declare no competing financial interests.

Author contributions
M.M. carried out most of the experiments. C.F.K. performed the 3D reconstruction of the external ear. S.D. generated the *Rosa*$^{(lox\text{-}stop\text{-}lox)Hoxa2\text{-}IRES\text{-}EGFP}$ allele. S.A. carried out ChIP/qPCR assays. N.V. performed some *in situ* hybridisation experiments. T.K., H.K. and N.B. contributed to data analysis and discussion as well as sharing unpublished results. F.M.R. and M.M. designed the experiments, analysed the data and wrote the manuscript.

Supplementary material
Supplementary material available online at
http://dev.biologists.org/lookup/suppl/doi:10.1242/dev.098046/-/DC1

References
Abdelhak, S., Kalatzis, V., Heilig, R., Compain, S., Samson, D., Vincent, C., Weil, D., Cruaud, C., Sahly, I., Leibovici, M. et al. (1997). A human homologue of the Drosophila eyes absent gene underlies branchio-oto-renal (BOR) syndrome and identifies a novel gene family. *Nat. Genet.* **15**, 157-164.
Alasti, F. and Van Camp, G. (2009). Genetics of microtia and associated syndromes. *J. Med. Genet.* **46**, 361-369.
Alasti, F., Sadeghi, A., Sanati, M. H., Farhadi, M., Stollar, E., Somers, T. and Van Camp, G. (2008). A mutation in HOXA2 is responsible for autosomal-recessive microtia in an Iranian family. *Am. J. Hum. Genet.* **82**, 982-991.
Baschek, V., Steinert, W. and Hildebrant, L. (2006). External ear duplication, a rare branchial arch abnormality. *Laryngorhinootologie* **85**, 861.
Caubit, X., Coré, N., Boned, A., Kerridge, S., Djabali, M. and Fasano, L. (2000). Vertebrate orthologues of the Drosophila region-specific patterning gene teashirt. *Mech. Dev.* **91**, 445-448.
Couly, G., Grapin-Botton, A., Coltey, P., Ruhin, B. and Le Douarin, N. M. (1998). Determination of the identity of the derivatives of the cephalic neural crest: incompatibility between Hox gene expression and lower jaw development. *Development* **125**, 3445-3459.
Danielian, P. S., Muccino, D., Rowitch, D. H., Michael, S. K. and McMahon, A. P. (1998). Modification of gene activity in mouse embryos in utero by a tamoxifen-inducible form of Cre recombinase. *Curr. Biol.* **8**, 1323-1326.
Donaldson, I. J., Amin, S., Hensman, J. J., Kutejova, E., Rattray, M., Lawrence, N., Hayes, A., Ward, C. M. and Bobola, N. (2012). Genome-wide occupancy links Hoxa2 to Wnt-β-catenin signaling in mouse embryonic development. *Nucleic Acids Res.* **40**, 3990-4001.
Dupé, V., Davenne, M., Brocard, J., Dollé, P., Mark, M., Dierich, A., Chambon, P. and Rijli, F. M. (1997). In vivo functional analysis of the Hoxa-1 3′ retinoic acid response element (3′RARE). *Development* **124**, 399-410.
Gendron-Maguire, M., Mallo, M., Zhang, M. and Gridley, T. (1993). Hoxa-2 mutant mice exhibit homeotic transformation of skeletal elements derived from cranial neural crest. *Cell* **75**, 1317-1331.
Gore, S. M., Myers, S. R. and Gault, D. (2006). Mirror ear: a reconstructive technique for substantial tragal anomalies or polyotia. *J. Plast. Reconstr. Aesthet. Surg.* **59**, 499-504.
Grammatopoulos, G. A., Bell, E., Toole, L., Lumsden, A. and Tucker, A. S. (2000). Homeotic transformation of branchial arch identity after Hoxa2 overexpression. *Development* **127**, 5355-5365.
Heldin, C. H. and Moustakas, A. (2012). Role of Smads in TGFβ signaling. *Cell Tissue Res.* **347**, 21-36.
Hogan, B. L., Blessing, M., Winnier, G. E., Suzuki, N. and Jones, C. M. (1994). Growth factors in development: the role of TGF-beta related polypeptide signalling molecules in embryogenesis. *Dev.* Suppl. **1994**, 53-60.
Horbelt, D., Denkis, A. and Knaus, P. (2012). A portrait of Transforming Growth Factor β superfamily signalling: background matters. *Int. J. Biochem. Cell Biol.* **44**, 469-474.
Hunter, A. G. and Yotsuyanagi, T. (2005). The external ear: more attention to detail may aid syndrome diagnosis and contribute answers to embryological questions. *Am. J. Med. Genet.* **135A**, 237-250.
Jakubíková, J., Staník, R. and Staníková, A. (2005). Malformations of the first branchial cleft: duplication of the external auditory canal. *Int. J. Pediatr. Otorhinolaryngol.* **69**, 255-261.
Kagurasho, M., Yamada, S., Uwabe, C., Kose, K. and Takakuwa, T. (2012). Movement of the external ear in human embryo. *Head Face Med.* **8**, 2.
King, J. A., Marker, P. C., Seung, K. J. and Kingsley, D. M. (1994). BMP5 and the molecular, skeletal, and soft-tissue alterations in short ear mice. *Dev. Biol.* **166**, 112-122.
Kingsley, D. M., Bland, A. E., Grubber, J. M., Marker, P. C., Russell, L. B., Copeland, N. G. and Jenkins, N. A. (1992). The mouse short ear skeletal morphogenesis locus is associated with defects in a bone morphogenetic member of the TGF beta superfamily. *Cell* **71**, 399-410.
Klockars, T. and Rautio, J. (2009). Embryology and epidemiology of microtia. *Facial Plast. Surg.* **25**, 145-148.
Kochhar, A., Fischer, S. M., Kimberling, W. J. and Smith, R. J. (2007). Branchio-oto-renal syndrome. *Am. J. Med. Genet. A* **143A**, 1671-1678.
Köntges, G. and Lumsden, A. (1996). Rhombencephalic neural crest segmentation is preserved throughout craniofacial ontogeny. *Development* **122**, 3229-3242.
Kountakis, S. E., Helidonis, E. and Jahrsdoerfer, R. A. (1995). Microtia grade as an indicator of middle ear development in aural atresia. *Arch. Otolaryngol. Head Neck Surg.* **121**, 885-886.
Ku, P. K., Tong, M. C. and Yue, V. (1998). Polyotia – a rare external ear anomaly. *Int. J. Pediatr. Otorhinolaryngol.* **46**, 117-120.
Kulessa, H. and Hogan, B. L. (2002). Generation of a loxP flanked bmp4loxP-lacZ allele marked by conditional lacZ expression. *Genesis* **32**, 66-68.
Kuratani, S. (2005). Craniofacial development and the evolution of the vertebrates: the old problems on a new background. *Zoolog. Sci.* **22**, 1-19.
Lobe, C. G., Koop, K. E., Kreppner, W., Lomeli, H., Gertsenstein, M. and Nagy, A. (1999). Z/AP, a double reporter for cre-mediated recombination. *Dev. Biol.* **208**, 281-292.
Madisen, L., Zwingman, T. A., Sunkin, S. M., Oh, S. W., Zariwala, H. A., Gu, H., Ng, L. L., Palmiter, R. D., Hawrylycz, M. J., Jones, A. R. et al. (2010). A robust and high-throughput Cre reporting and characterization system for the whole mouse brain. *Nat. Neurosci.* **13**, 133-140.
Mallo, M. and Gridley, T. (1996). Development of the mammalian ear: coordinate regulation of formation of the tympanic ring and the external acoustic meatus. *Development* **122**, 173-179.
Mark, M., Lohnes, D., Mendelsohn, C., Dupé, V., Vonesch, J. L., Kastner, P., Rijli, F., Bloch-Zupan, A. and Chambon, P. (1995). Roles of retinoic acid receptors and of Hox genes in the patterning of the teeth and of the jaw skeleton. *Int. J. Dev. Biol.* **39**, 111-121.
Martin, J. F., Bradley, A. and Olson, E. N. (1995). The paired-like homeo box gene MHox is required for early events of skeletogenesis in multiple lineages. *Genes Dev.* **9**, 1237-1249.
Meyer, L. R., Zweig, A. S., Hinrichs, A. S., Karolchik, D., Kuhn, R. M., Wong, M., Sloan, C. A., Rosenbloom, K. R., Roe, G., Rhead, B. et al. (2013). The UCSC Genome Browser database: extensions and updates 2013. *Nucleic Acids Res.* **41**, D64-D69.
Miguez, A., Ducret, S., Di Meglio, T., Parras, C., Hmidan, H., Haton, C., Sekizar, S., Mannioui, A., Vidal, M., Kerever, A. et al. (2012). Opposing roles for Hoxa2 and Hoxb2 in hindbrain oligodendrocyte patterning. *J. Neurosci.* **32**, 17172-17185.
Minoux, M. and Rijli, F. M. (2010). Molecular mechanisms of cranial neural crest cell migration and patterning in craniofacial development. *Development* **137**, 2605-2621.
Minoux, M., Antonarakis, G. S., Kmita, M., Duboule, D. and Rijli, F. M. (2009). Rostral and caudal pharyngeal arches share a common neural crest ground pattern. *Development* **136**, 637-645.
Mishra, S. C. and Misra, M. (1978). Mirror image pinna. *J. Laryngol. Otol.* **92**, 709-711.
Oury, F., Murakami, Y., Renaud, J. S., Pasqualetti, M., Charnay, P., Ren, S. Y. and Rijli, F. M. (2006). Hoxa2- and rhombomere-dependent development of the mouse facial somatosensory map. *Science* **313**, 1408-1413.
Pan, B., Qie, S., Zhao, Y., Tang, X., Lin, L., Yang, Q., Zhuang, H. and Jiang, H. (2010). Surgical management of polyotia. *J. Plast. Reconstr. Aesthet. Surg.* **63**, 1283-1288.
Pasqualetti, M., Ori, M., Nardi, I. and Rijli, F. M. (2000). Ectopic Hoxa2 induction after neural crest migration results in homeosis of jaw elements in Xenopus. *Development* **127**, 5367-5378.
Pasqualetti, M., Ren, S. Y., Poulet, M., LeMeur, M., Dierich, A. and Rijli, F. M. (2002). A Hoxa2 knockin allele that expresses EGFP upon conditional Cre-mediated recombination. *Genesis* **32**, 109-111.
Passos-Bueno, M. R., Ornelas, C. C. and Fanganiello, R. D. (2009). Syndromes of the first and second pharyngeal arches: A review. *Am. J. Med. Genet. A* **149A**, 1853-1859.
Porter, C. J. and Tan, S. T. (2005). Congenital auricular anomalies: topographic anatomy, embryology, classification, and treatment strategies. *Plast. Reconstr. Surg.* **115**, 1701-1712.
Qian, D., Jones, C., Rzadzinska, A., Mark, S., Zhang, X., Steel, K. P., Dai, X. and Chen, P. (2007). Wnt5a functions in planar cell polarity regulation in mice. *Dev. Biol.* **306**, 121-133.
Ren, S. Y., Pasqualetti, M., Dierich, A., Le Meur, M. and Rijli, F. M. (2002). A Hoxa2 mutant conditional allele generated by Flp- and Cre-mediated recombination. *Genesis* **32**, 105-108.
Rijli, F. M., Mark, M., Lakkaraju, S., Dierich, A., Dollé, P. and Chambon, P. (1993). A homeotic transformation is generated in the rostral branchial region

of the head by disruption of Hoxa-2, which acts as a selector gene. *Cell* **75**, 1333-1349.
Santagati, F. and Rijli, F. M. (2003). Cranial neural crest and the building of the vertebrate head. *Nat. Rev. Neurosci.* **4**, 806-818.
Santagati, F., Minoux, M., Ren, S. Y. and Rijli, F. M. (2005). Temporal requirement of Hoxa2 in cranial neural crest skeletal morphogenesis. *Development* **132**, 4927-4936.
Schoenwolf, G. C. and Larsen, W. J. (2009). *Larsen's Human Embryology*, 4th edn. Philadelphia, PA: Elsevier/Churchill Livingstone.
Solloway, M. J. and Robertson, E. J. (1999). Early embryonic lethality in Bmp5;Bmp7 double mutant mice suggests functional redundancy within the 60A subgroup. *Development* **126**, 1753-1768.
Takechi, M. and Kuratani, S. (2010). History of studies on mammalian middle ear evolution: a comparative morphological and developmental biology perspective. *J. Exp. Zool.* **314B**, 417-433.
ten Berge, D., Brouwer, A., Korving, J., Martin, J. F. and Meijlink, F. (1998). Prx1 and Prx2 in skeletogenesis: roles in the craniofacial region, inner ear and limbs. *Development* **125**, 3831-3842.
Winnier, G., Blessing, M., Labosky, P. A. and Hogan, B. L. (1995). Bone morphogenetic protein-4 is required for mesoderm formation and patterning in the mouse. *Genes Dev.* **9**, 2105-2116.
Wood-Jones, F. and I-Chuan, W. (1934). The development of the external ear. *J. Anat.* **68**, 525-533.
Xu, P. X., Adams, J., Peters, H., Brown, M. C., Heaney, S. and Maas, R. (1999). Eya1-deficient mice lack ears and kidneys and show abnormal apoptosis of organ primordia. *Nat. Genet.* **23**, 113-117.
Zakin, L. and De Robertis, E. M. (2004). Inactivation of mouse Twisted gastrulation reveals its role in promoting Bmp4 activity during forebrain development. *Development* **131**, 413-424.

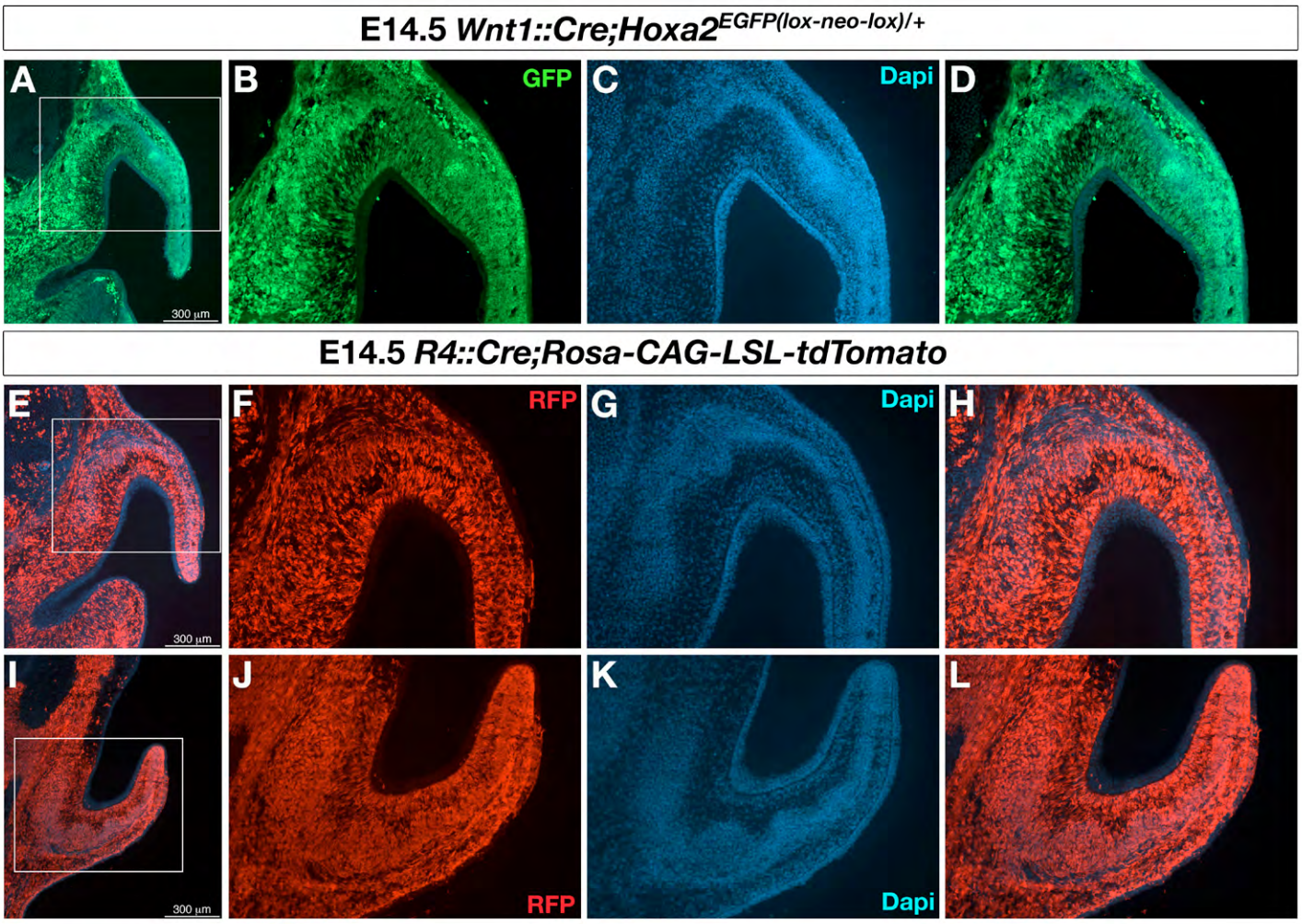

Fig. S1. Fate mapping of neural crest-derived pinna. (A-L) Anti-EGFP (A, B, D) and anti-RFP (E, F, H, I, J, L) immunostaining and DAPI staining (A, C, D, E, G, H, I, K, L) on frontal (A-D, E-H) and horizontal (I-L) sections through the external ear of E14.5 *Wnt1::Cre;Hoxa2*$^{EGFP(lox\text{-}neo\text{-}lox)/+}$ (A-D) and *R4::Cre;Rosa-CAG-LSL-tdTomato* (E-L) fetuses. In A and D, E and H, I and L, DAPI and anti-EGFP (A, D) or DAPI and anti-RFP (E, H, I, L) stainings are merged. B-D, F-H and J-L are higher magnifications of the domains outlined in A, E and I, respectively.

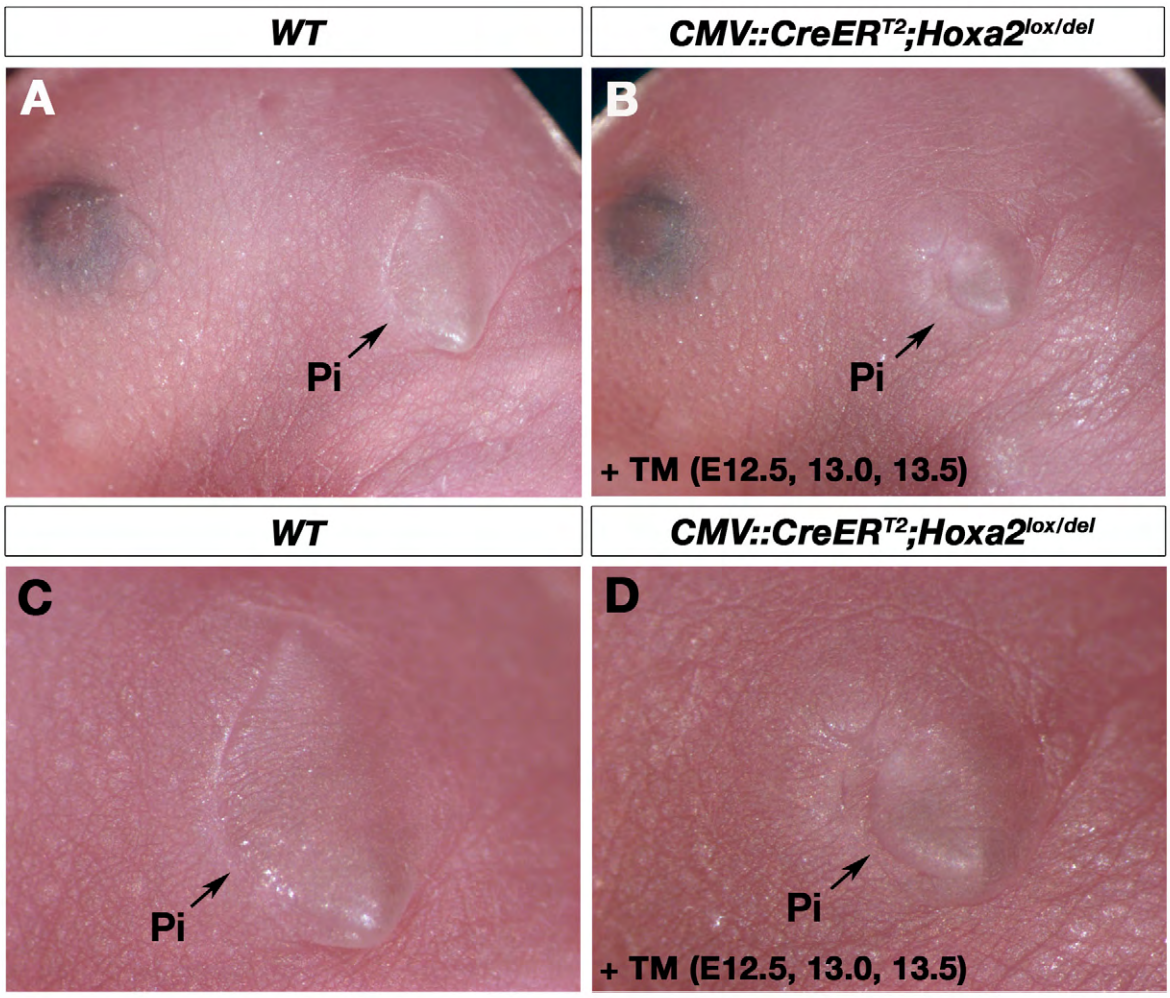

Fig. S2. Temporal requirement of Hoxa2 in pinna morphogenesis. (A-D) Lateral views of the head of E18.5 *wild-type* (*WT*) (A, C) and *CMV::CreER^{T2};Hoxa2$^{lox/del}$* mutant fetuses treated with tamoxifen (TM) at E12.5, E13.0 and E13.5 (B, D). C and D are enlarged views of pinnae (arrows, Pi) in A and B, respectively. Note the small pinna resulting from late Hoxa2 downregulation (B, D).

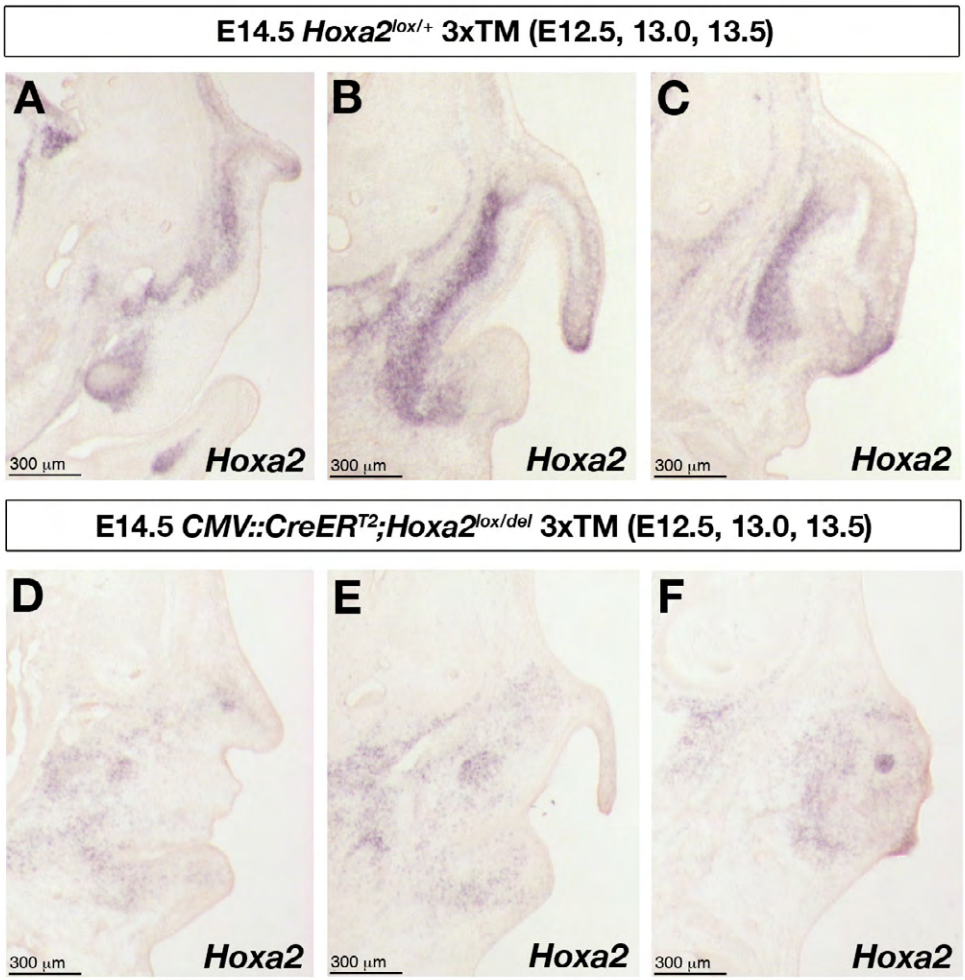

Fig. S3. Loss of *Hoxa2* expression in TM-treated mutants. (A-F) *Hoxa2 in situ* hybridization on frontal sections through the external ear of E14.5 *Hoxa2*$^{lox/+}$ control (A-C) and *CMV::CreER*^{T2}*;Hoxa2*$^{lox/del}$ mutant (D-F) fetuses treated with tamoxifen (TM) at E12.5, E13.0 and E13.5. Top is dorsal, bottom is ventral and sections are from anterior to posterior. Note the significant downregulation of *Hoxa2* expression in D-F.

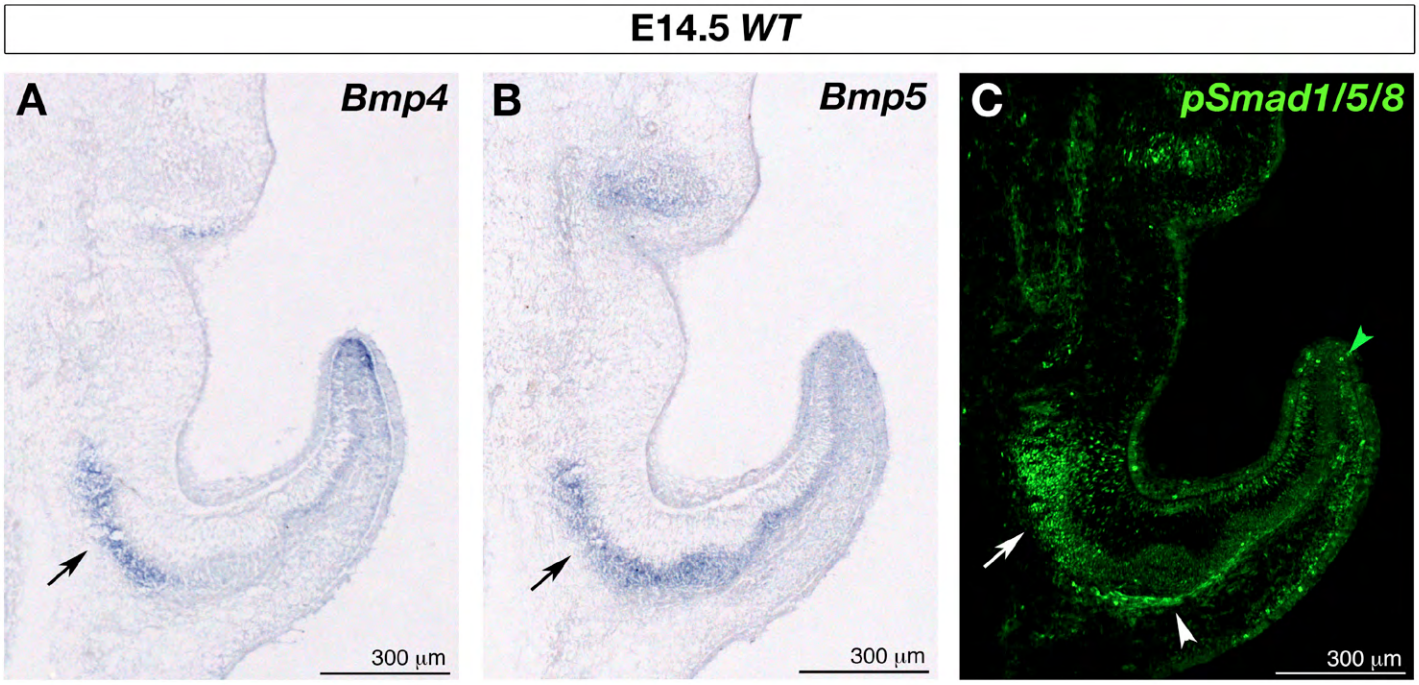

Fig. S4. Distribution of phosphoSmad1/5/8, *Bmp4* and *Bmp5* expression in the developing pinna. (A-C) *Bmp4* (A) and *Bmp5* (B) *in situ* hybridization and anti-phosphoSmad1/5/8 antibody immunostaining (C) on adjacent horizontal sections through the external ear of E14.5 *wild-type* (*WT*) fetuses. Black arrows in A and B, and the white arrow in C show *Bmp4*, *Bmp5* and phosphoSmad1/5/8 positive cells at the base the pinna. The white arrowhead in C shows the Eya1^{+} subpopulation of phosphoSmad1/5/8 positive cells next to the pinna mesenchymal core of *Bmp5* expression. The green arrowhead in C shows phosphoSmad1/5/8 activated cells at the tip of the pinna, just beneath the ectoderm. Top is anterior, bottom is posterior.

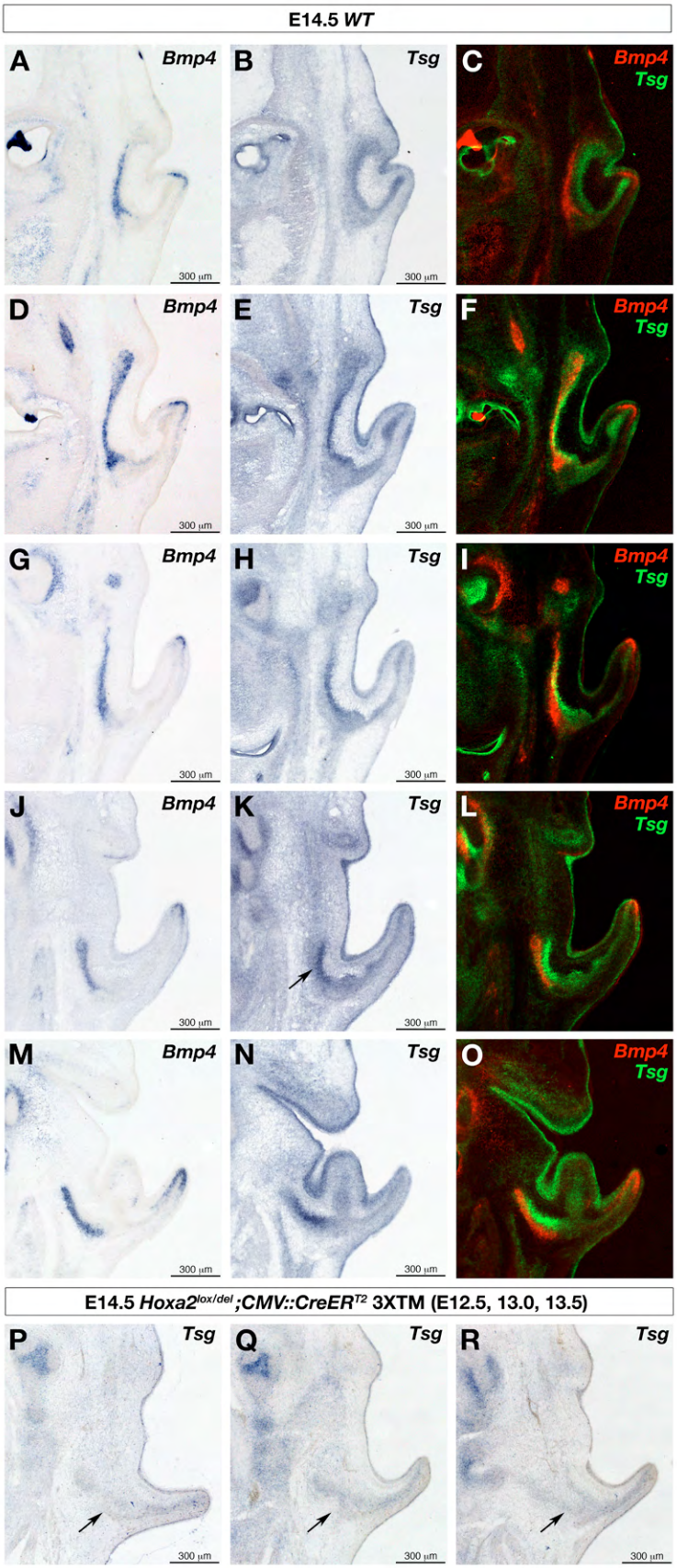

Fig. S5. Hoxa2 positively regulates *Tsg*. (A-O) *In situ* hybridization on adjacent horizontal sections through the external ear of E14.5 *wild-type* (*WT*) fetuses using *Bmp4* (A, D, G, J, M) and *Tsg* (B, E, H, K, N) probes. A merge between adjacent sections hybridised with *Bmp4* and *Tsg*, respectively (C, F, I, L, O) reveals that *Tsg* is highly expressed directly adjacent to the *Bmp4* positive domain. (P-R) *Tsg in situ* hybridization on horizontal sections through the external ear of E14.5 *CMV::CreER^{T2};Hoxa2$^{lox/del}$* mutant fetuses treated with tamoxifen (TM) at E12.5, E13.0 and E13.5. Top is anterior, bottom is posterior.

Fig. S6. Validation by qPCR of Hoxa2 binding at *Bmp4* and *Bmp5* non-coding regions. (A) Fold enrichment of Hoxa2 over IgG negative control antibody (Neg Ab) is shown for each Hoxa2-bound region. Values correspond to the average of duplicate samples and are representative of two independent experiments. Itih4 is a negative control gene (unbound region). The numbers in brackets correspond to the FDR (False Discovery Rate) of each bound region in Hoxa2 ChIP-seq (Donaldson et al., 2012). (B) Sequence alignment and conservation of Hoxa2-bound regions across Vertebrates, provided by the UCSC browser (Meyer et al., 2013).

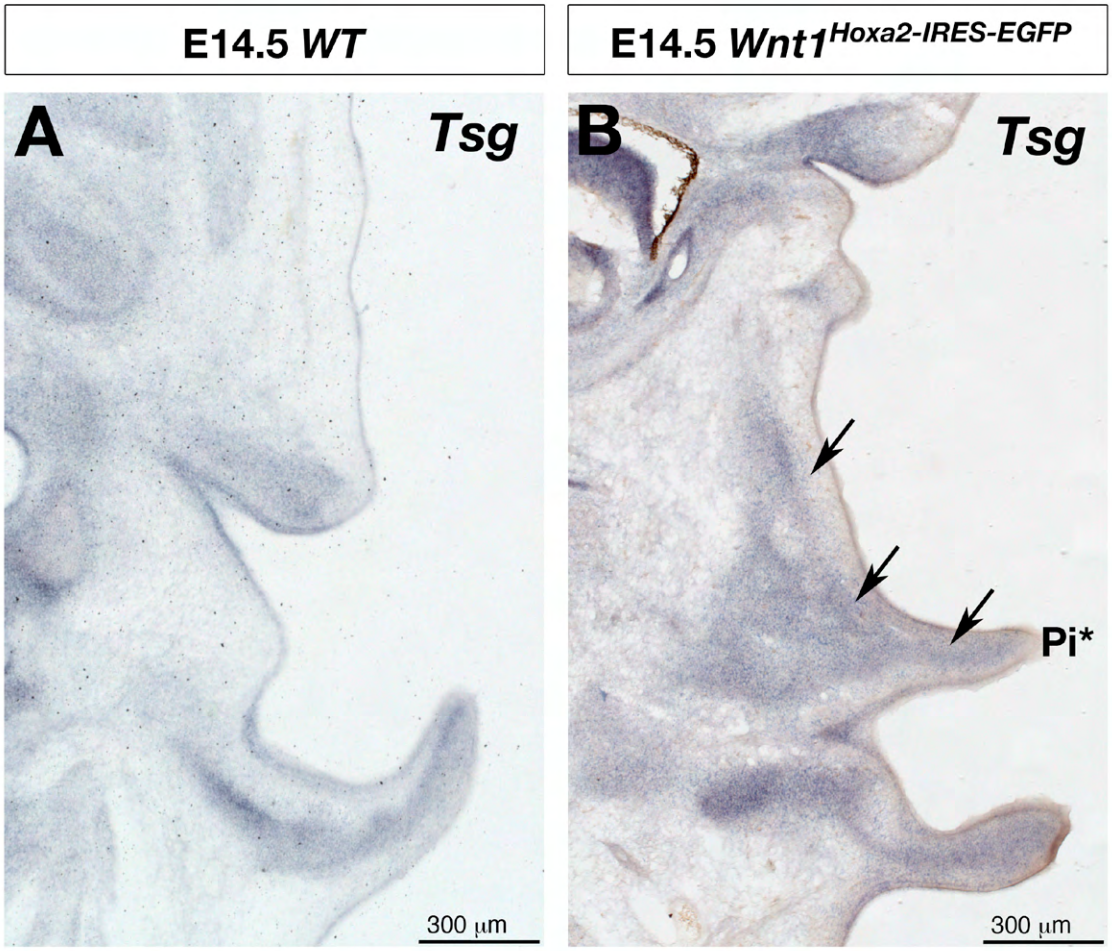

Fig. S7. *Tsg* is ectopically expressed in the Hoxa2-induced duplicated pinna. (A, B) *Tsg in situ* hybridization performed on horizontal sections through the external ear of E14.5 *Wild type* (*WT*) (A) and *Wnt1*$^{Hoxa2\text{-}IRES\text{-}EGFP}$ mutant (B) fetuses. Top is anterior, bottom is posterior. The black arrows indicate *Tsg* ectopic expression in the duplicated pinna (Pi*) and more anteriorly.